Fault-based Probabilistic Seismic Hazard Analysis in Regions with Low Strain Rates and a Thick Seismogenic Layer: A Case Study from Malawi

Jack Williams (jack.williams@otago.ac.nz)
University of Otago https://orcid.org/0000-0001-6669-308X
Maximillian Werner
University of Bristol School of Earth Sciences
Katsuichiro Goda
Western University
Luke Wedmore
University of Bristol School of Earth Sciences
Raffaele De Risi
University of Bristol Faculty of Engineering
Juliet Biggs
University of Bristol School of Earth Sciences
Hassan Mdala
Malawi Geological Survey
Zuze Dulanya
University of Malawi Chancellor College
Åke Fagereng
Cardiff University
Felix Mphepo
Malawi Geological Survey
Patrick Chindandali
Malawi Geological Survey

Research Article

Keywords: probabilistic seismic hazard analysis, East African Rift, 49 Malawi, earthquake fault source

Posted Date: March 28th, 2022

DOI: https://doi.org/10.21203/rs.3.rs-1452299/v1

Fault-based probabilistic seismic hazard analysis in regions with low strain rates and a thick seismogenic layer: a case study from Malawi

Jack Williams[1,2,3*], Maximillian Werner[1], Katsuichiro Goda[4], Luke Wedmore[1], Raffaele De Risi[5], Juliet Biggs[1], Hassan Mdala[6], Zuze Dulanya[7], Åke Fagereng[2], Felix Mphepo[6] and Patrick Chindandali[8]

[1]School of Earth Sciences, University of Bristol, Bristol, UK.
[2]School of Earth and Environmental Sciences, Cardiff University, Cardiff, UK.
[3]Department of Geology, University of Otago, Dunedin, New Zealand.
[4]Department of Earth Sciences, Western University, London, Ontario, Canada.
[5]Department of Civil Engineering, University of Bristol, Bristol, UK.
[6]Geological Survey Department, Mzuzu, Malawi.
[7]Geography and Earth Sciences Department, University of Malawi, Zomba, Malawi.
[8]Geological Survey Department, Zomba, Malawi.

*Corresponding author. E-mail: jack.williams@otago.ac.nz;

Abstract

In low strain rate regions, extrapolation of incomplete instrumental earthquake records is a limitation for probabilistic seismic hazard analysis (PSHA). This limitation can be addressed by incorporating geologic and geodetic data into fault-based seismogenic sources, although it is not always clear how on-fault magnitude-frequency distributions should be described and, if the seismogenic layer is especially thick, how these

sources should be extrapolated down-dip. We explore these issues in the context of a new PSHA for Malawi, where regional extensional rates are 0.5-2 mm/yr, the seismogenic layer is 30-40 km thick, the instrumental catalog is ∼60 years long, and fault-based sources were recently collated in the Malawi Seismogenic Source Database. Furthermore, Malawi is one of several countries along the East African Rift where exposure to seismic hazard is growing, but PSHA typically considers instrumental records alone. We use stochastic event catalogs to explore different fault-source down-dip extents and magnitude-frequency distributions. These indicate that hazard levels are highest for a Gutenberg-Richter on-fault magnitude-frequency distribution, even at low probabilities of exceedance (2% in 50 years), whilst seismic hazard levels are also sensitive to how relatively short (<50 km) fault sources are extrapolated down-dip. For sites close to fault sources (<40 km), seismic hazard levels are doubled compared to previous instrumental-seismicity based PSHA in Malawi. Cumulatively, these results highlight the need for careful fault source modelling in PSHA of low strain rate regions, and the need for new fault-based PSHA elsewhere in East Africa.

Keywords: probabilistic seismic hazard analysis, East African Rift, Malawi, earthquake fault source

1 Introduction

In regions with low slip rate faults (∼0.1-10 mm/yr; C. H. Scholz et al., 1986), the typical recurrence time for moderate-large magnitude earthquakes (∼1000-100,000 yrs) is greater than the length of instrumental earthquake catalogs (∼50-100 years). Therefore probabilistic seismic hazard analysis (PSHA) typically requires extrapolating catalogs beyond their duration (e.g., Zahran et al., 2015; Goitom et al., 2017; Poggi et al., 2017), and/or combining geologic and geodetic data into fault-based seismogenic sources (e.g., Stirling et al., 2012; Petersen et al., 2015). In the former case, there are challenges with defining the maximum expected earthquake magnitude for the assessed region (Holschneider et al., 2011) and accounting for catalog declustering when developing areal or smoothed seismicity source models (Helmstetter & Werner, 2012; Stein et al., 2012; Wang et al., 2021). PSHA using fault-based sources is therefore increasingly popular, and in particular, the use of inversion techniques that constrain on-fault magnitude-frequency distributions (MFDs) by balancing geodetic, geologic, and seismological data (Field et al., 2014, 2021; Geist & Parsons, 2018; Chartier et al., 2019). However, it is challenging to reconcile earthquake rates from these data in low strain rate (Cox et al., 2012; Hodge et al., 2015; Vallage & Bollinger, 2020), and yet it is these regions where estimated seismic hazard levels are particularly sensitive to assumptions about fault geometry and segmentation (Hodge et al., 2015; DuRoss et al., 2016;

Visini et al., 2020; Gómez-Novell et al., 2020; Valentini et al., 2020; Goda & Sharipov, 2021).

The use of fault-based sources in PSHA requires extrapolating geologic and geodetic constraints on fault deformation through the Earth's crust. In particular, assumptions about a fault's down-dip extent influence its seismic moment rate and source-to-site distance in ground motion calculations. In most continental regions, the seismogenic layer is 10-20 km thick (e.g., Jackson et al., 2021), and the uncertainty of extrapolating surface fault data down-dip does not significantly influence hazard levels (Field et al., 2014). However, it is not clear whether uncertainty on fault down-dip extents will influence fault-based PSHA in regions where the seismogenic layer is much thicker (20-40 km), such as in the East African and Baikal rifts (Jackson & Blenkinsop, 1993; Nyblade & Langston, 1995; Déverchère et al., 2001; Lavayssière et al., 2019; Ebinger et al., 2019; Stevens et al., 2021).

In this study, we present a new fault-based PSHA for Malawi. Malawi is located within a 900 km-long amagmatic section of the Western Branch of the East African Rift (EAR), and provides an ideal case study to investigate PSHA in a low strain rate region with a thick seismogenic layer as: (1) geodetically-derived regional extension rates are low (0.5-2 mm/yr; Stamps et al., 2021; Wedmore et al., 2021), but nevertheless an order of magnitude higher than inferred from the last 50 years of instrumentally-recorded seismicity (Hodge et al., 2015; Ebinger et al., 2019), and (2) the seismogenic layer is ∼30-40 km thick (Jackson & Blenkinsop, 1993; Nyblade & Langston, 1995; Ebinger et al., 2019; Stevens et al., 2021; Craig & Jackson, 2021). Furthermore, constraints on the seismogenic potential of Malawi's active faults have improved with the collection of new geologic and geodetic data (Hodge et al., 2019; C. A. Scholz et al., 2020; Shillington et al., 2020; Wedmore, Williams, et al., 2020; Wedmore, Biggs, et al., 2020; Wedmore et al., 2021; Williams, Wedmore, Scholz, et al., 2021a; Kolawole et al., 2021), which have been synthesised for seismic hazard analysis in the Malawi Seismogenic Source Database (MSSD; Williams, Wedmore, Fagereng, et al., 2021a) .

Malawi is also one of several countries along the EAR where seismic risk is being exacerbated by population growth and the development of seismically vulnerable building stock (Meghraoui et al., 2016; Goda et al., 2016; Poggi et al., 2017; World-Bank, 2019; Kloukinas et al., 2020; Giordano et al., 2021). However, PSHA in the EAR typically considers only the instrumental record of seismicity (e.g., Midzi et al., 1999; Bwambale et al., 2016; Delvaux et al., 2017; Goitom et al., 2017; Delvaux et al., 2017; Poggi et al., 2017; Tuluka et al., 2020; Msabi & Ferdinand, 2021). Here, we incorporate the MSSD into a PSHA for Malawi through stochastic event catalogs (Musson, 1999; Atkinson & Goda, 2013) to provide critical inputs for assessing Malawi's increasing seismic risk (Goda et al., 2016, 2021), and examine how fault-based sources could be used in future PSHA elsewhere in East Africa.

2 Background to seismic hazard assessment in Malawi

2.1 The seismotectonic setting of Malawi

Malawi's national borders are closely aligned to a 900 km long section of the East African Rift's Western Branch, with earthquakes $M_W > 4.5$ and active faults > 50 km long documented throughout (Fig. 1; Dixey, 1926; Ebinger, Rosendahl, & Reynolds, 1987; Specht & Rosendahl, 1989; Chapola & Kaphwiyo, 1992; Poggi et al., 2017; Wedmore, Biggs, et al., 2020; Williams, Wedmore, Scholz, et al., 2021a). In central and northern Malawi, the EAR has mostly been flooded by Lake Malawi, whilst in southern Malawi the rift is onshore and at its southern end has intersected and reactivated Karoo (i.e., Triassic-Jurassic) age faults in the Lower Shire Basin (Dulanya, 2017; Wedmore, Williams, et al., 2020; Williams, Mdala, et al., 2021; Kolawole et al., 2021). Only negligible amounts of melt have been detected in Malawi's crust (Njinju et al., 2019; Accardo et al., 2020; Hopper et al., 2020), and so rift extension is primarily accommodated by normal fault earthquakes (Biggs et al., 2010; Hodge et al., 2015; Williams, Wedmore, Fagereng, et al., 2021a).

The most comprehensive instrumental record of earthquakes in Malawi is the Sub-Saharan Africa Global Earthquake Model (SSA-GEM) catalog (Fig. 1a; Poggi et al., 2017). This was mainly developed from the International Seismological Centre (ISC) catalog, which in Malawi is complete since 1965 for events $M_W > 4.5$ (Hodge et al., 2015). Within this record, two events stand out: the 1989 M_W 6.3 Salima Earthquake (Jackson & Blenkinsop, 1993; Gupta & Malomo, 1995) and the 2009 Karonga earthquake sequence (Biggs et al., 2010; Hamiel et al., 2012; Macheyeki et al., 2015; Gaherty et al., 2019). The former was assigned a VIII on the Modified Mercalli Intensity Scale (MMI; Gupta & Malomo, 1995), and its 32 ± 5 km focal depth is typical of Malawi's 30-40 km thick seismogenic layer (Nyblade & Langston, 1995; Craig & Jackson, 2021; Ebinger et al., 2019; Stevens et al., 2021). In contrast, the Karonga earthquake sequence primarily consistent of 4 shallow (focal depths 5-10 km) M_W 5.5−5.9 events over 13 days (Biggs et al., 2010) and resulted in a 9-18 km long surface rupture along the previously unrecognised St Mary Fault (Macheyeki et al., 2015). Focal mechanism stress inversions indicate a normal fault stress state in Malawi with an ENE-WSW trending minimum principal compressive stress (Delvaux & Barth, 2010; Ebinger et al., 2019; Williams et al., 2019).

2.2 Previous seismic hazard assessment in Malawi

In a PSHA for Malawi that considered areal sources developed from the SSA-GEM catalog, Poggi et al. (2017) found that for peak ground acceleration (PGA) there is a 10% probability of exceeding (PoE) 0.10-0.15 g in 50 years. Hazard levels were relatively uniform across Malawi in this study as it was part of a single ∼380,000 km^2 areal source zone that extends from Mozambique to southern Tanzania. However, geodetic models indicate that extension

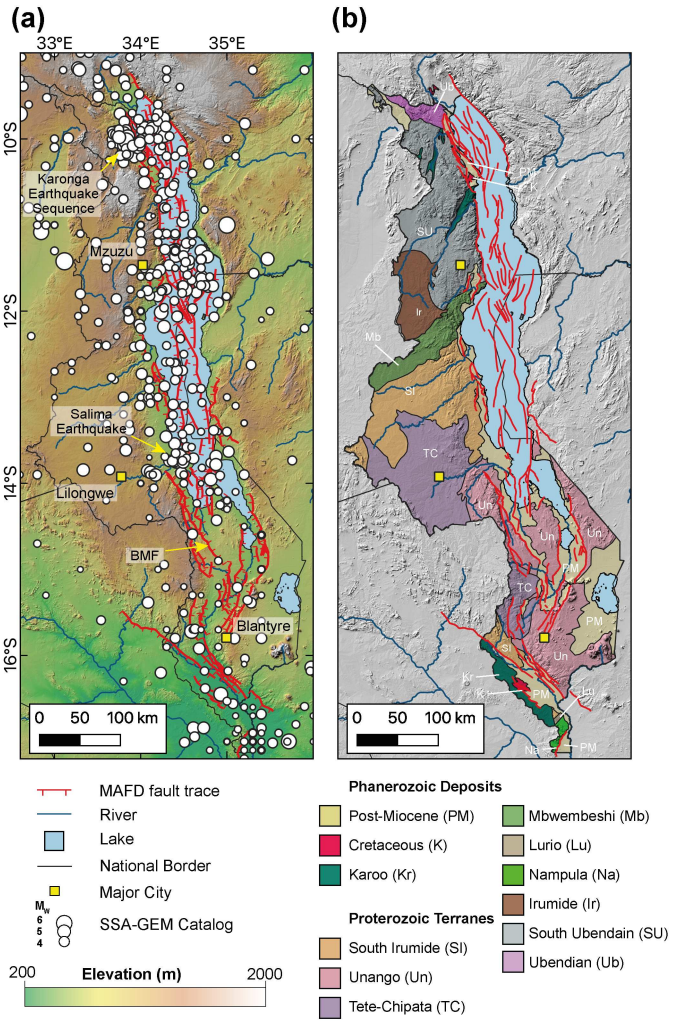

Fig. 1 Map of Malawi in the context of: (a) the Malawi Active Fault Database (MAFD; Williams, Wedmore, Scholz, et al., 2021a) and the Sub-Saharan Africa Global Earthquake Model (SSA-GEM) catalog (Poggi et al., 2017), and (b) regional geological terranes (Fullgraf et al., 2017). BMF; Bilila-Mtakataka Fault.

rates increase from south to north Malawi (Saria et al., 2014; Stamps et al., 2021; Wedmore et al., 2021), and there are also geologic observations of across-rift variations in fault activity (Accardo et al., 2018; Shillington et al., 2020; Wedmore, Biggs, et al., 2020). These spatial variations in deformation were incorporated into a PSHA by Hodge et al. (2015), who developed seven fault-based seismogenic sources in Malawi from previously mapped major rift-bounding faults in Malawi and geodetically-derived regional extension rates (Stamps et al., 2008). Inclusion of these sources into PSHA resulted

in higher hazard levels adjacent to these faults (10% PoE 0.15-0.25 g in 50 years vs. 10% PoE 0.10-15 g in 50 years in Poggi et al. (2017)), with these increases greatest for cases that inferred relatively frequent, moderate magnitude ruptures of shorter discrete fault segments, rather than rarer, larger magnitude earthquakes spanning entire faults. This PSHA was later incorporated into a quantitative seismic risk assessment for Malawi (Goda et al., 2016), and a scenario-based risk assessment for the region around the Bilila-Mtakataka Fault in southern Malawi (Fig. 1a; Goda et al., 2021). These studies estimated that in a worst case M_W 7.8 earthquake along the entire fault, ∼160,000-440,000 buildings would collapse (Goda et al., 2021) .

Since 2015, high resolution digital elevation models (Hodge et al., 2019, 2020; Wedmore, Williams, et al., 2020; Wedmore, Biggs, et al., 2020), aeromagnetic and gravity data (Kolawole et al., 2018, 2021; Chisenga et al., 2019), and a new generation of seismic reflection data in Lake Malawi (Shillington et al., 2016, 2020; C. A. Scholz et al., 2020) have led to significant advances in the identification and mapping of active faults in Malawi. These datasets were combined into the Malawi Active Fault Database (MAFD), a geospatial database for 113 faults that are inferred to be active in Malawi and neighbouring areas of Mozambique and Tanzania (Williams, Wedmore, Scholz, et al., 2021a, 2021b). In addition, new constraints on fault slip rates in Malawi have been provided from new geodetic data (Stamps et al., 2018; Wedmore et al., 2021) and the fault offsets of a 75 Ka. reflector in seismic reflection data in Lake Malawi (Shillington et al., 2020). These new geologic and geodetic data were combined into the Malawi Seismogenic Source Database (MSSD), a database that provides slip rate, earthquake magnitudes and recurrence interval estimates of faults included in the MAFD (Williams, Wedmore, Fagereng, et al., 2021a, 2021b).

3 PSHA Workflow

Here we use the MSSD and previously defined EAR areal sources (Poggi et al., 2017) to develop a new PSHA for Malawi. We incorporate the MSSD by considering both the earthquake magnitude and recurrence interval assigned to each MSSD source (the 'Direct MSSD' approach), and a moment rate balancing approach that explicitly explores different hypotheses for the down-dip extent of the MSSD sources and whether they exhibit Gutenberg-Richter or characteristic magnitude-frequency distributions (the 'Adapted MSSD' approach; Youngs & Coppersmith, 1985; Convertito et al., 2006). These different MSSD interpretations are realised in five stochastic event catalogs, with off-fault events considered using an areal source based catalog. The PSHA is then formulated by evaluating these five catalogs using four ground motion models (GMMs; Akkar et al., 2014; Boore et al., 2014; Chiou & Youngs, 2014; Atkinson & Adams, 2013). Hence, for a given site, PoE, and spectral acceleration, we calculate 20 ground motion intensity values. Following an ensemble approach,

we use the mean and distribution of these values to describe seismic hazard and its uncertainty (Marzocchi et al., 2015; Meletti et al., 2021).

Our analysis is performed for a rectangular region that bounds Malawi with a grid spacing of 0.2° (Fig. 1). For each grid point, we consider two values for the average shear wave velocity to 30 m depth (V_{S30}): (1) a reference site condition (V_{S30}=760 m/s), and (2) the value derived from the USGS V_{S30} database (Wald & Allen, 2007). In addition, we performed site specific PSHA for the three largest cities in Malawi: Lilongwe, Blantyre, and Mzuzu (Fig. 1a). We describe the earthquake sources and stochastic event catalogs further in Section 4, the GMMs in Section 5.1, and seismic hazard calculations in Section 5.2. PSHA results are presented in Section 6. A summary of our PSHA workflow is shown in Fig. 2. Abbreviations and symbols are listed in Table 1.

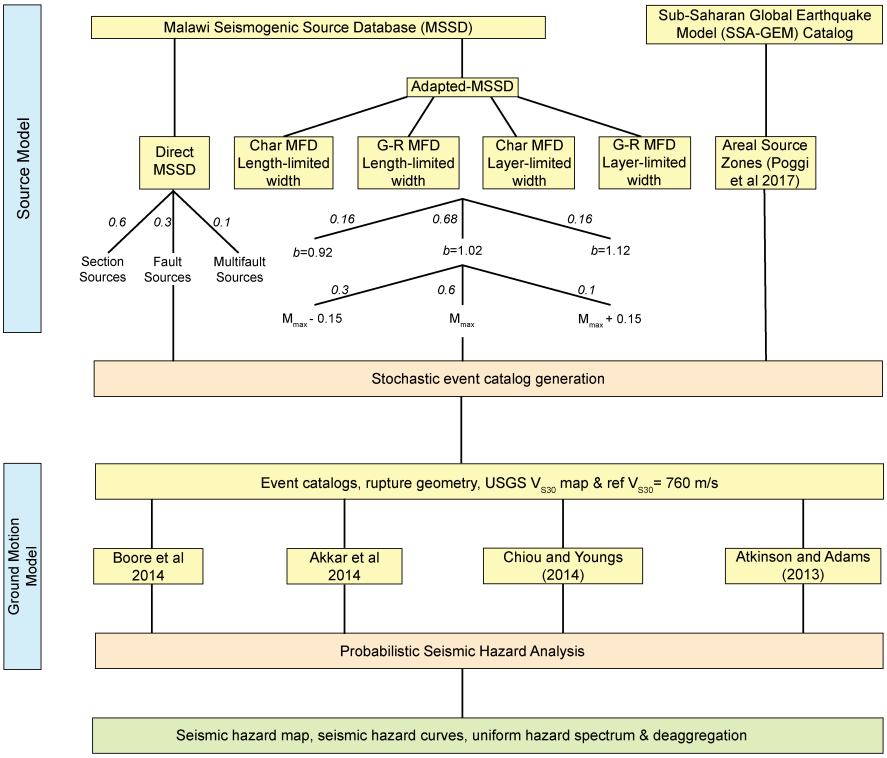

Fig. 2 Flow chart for the PSHA conducted in this study. Branches are equally weighted unless otherwise stated.

Table 1 List of acronyms and symbols used in this study

Acronym/Symbol	Definition
Acronyms	
CoV	Coefficient of Variation
EAR	East African Rift
G-R	Gutenberg-Richter
GMM	Ground motion model
GSRM	Global Strain Rate Model
MAFD	Malawi Active Fault Database
MMI	Modified Mercalli Intensity Scale
MPS19	Italian Seismic Hazard Model (Modello di Pericolosità Sismica)
MSSD	Malawi Seismogenic Source Database
MFD	Magnitude frequency distribution
PGA	Peak ground acceleration
PoE	Probability of exceedance
PSHA	Probabilistic seismic hazard analysis
SA	Spectral Acceleration
SHIFT	Seismic hazard inferred from tectonics
SSA-GEM	Sub-Sahara African Global Earthquake Model catalog
SSA-GSRM	Sub-Saharan African Geodetic Strain Rate Model
V_{S30}	Average shear wave velocity to 30 m depth
Symbols	
α_C	Activity rate for a characteristic MFD
α_{NC}	Activity rate for the non-characteristic magnitude range in a characteristic MFD
α_{GR}	Activity rate for a G-R MFD
β	The product of the b-value and ln10
δ_s	Source dip
Δm_1	Magnitude range in characteristic MFD where recurrence rate is less than characteristic portion
Δm_2	Magnitude range for characteristic events
λ_s	Annual occurrence rate for source events
μ	Crustal rigidity
A_s	Source area
c_1 & c_2	Empirical constants from Leonard (2010)
$\bar{D}_s$	Source single event displacement
$f_M(m)$	Source probability density function for magnitude m
L_s	Source length
m	Earthquake magnitude
M_{Max}	Maximum expected earthquake magnitude
M_0^{Max}	Seismic moment for M_{Max}
M_{min}	Minimum earthquake magnitude considered for the PSHA
$\dot{M}_0$	Seismic moment release rate
N	Number of event catalog-GMM combinations
R_s	Source recurrence interval
S_s	Source slip rate
t_s	Time to source's next event in stochastic catalog
ν_{GM}	Rate of ground motion exceedance
W_s	Source width
z	Seismogenic layer thickness

4 Source models

4.1 The Direct Approach to the Malawi Seismogenic Source Database

The MSSD is a geospatial database of 141 geometrically-defined section sources, 107 fault sources, and 27 multi-fault sources that were identified from the 113 faults contained within the MAFD. The number of faults in the MAFD and fault sources in the MSSD are not the same due to the requirement that source lengths are $\geq$5 km long, and that faults that splay in map view as considered to represent different sources. Further description of the MSSD is provided by Williams, Wedmore, Fagereng, et al. (2021a), and so we only briefly summarise the parameters of interest for PSHA here. An earthquake magnitude (m) and single event displacement ($\bar{D}_s$) is assigned to each source in the MSSD through the Leonard (2010) magnitude-area scaling relationships for interplate dip-slip faults. For these calculations, source width (W_s) is derived through:

$$W_s = \begin{cases} c_1 L_s^{\frac{2}{3}}, & \text{if } c_1 L_s^{\frac{2}{3}} \text{ is } < \frac{z}{\sin \delta_s} \\ \\ \frac{z}{\sin \delta}, & \text{if } c_1 L_s^{\frac{2}{3}} \text{ is } \geq \frac{z}{\sin \delta_s} \end{cases} \tag{1}$$

where c_1 is an empirically derived parameter and equals 17.5 $\mathrm{m}^{\frac{1}{3}}$ for interplate dip-slip faults (Leonard, 2010), z is the seismogenic layer thickness in Malawi, set to an intermediate estimate of 35 km (Ebinger et al., 2019; Stevens et al., 2021), and L_s and δ_s are source length and dip. If two sources intersect down-dip, the shorter source is assumed to be truncated by the longer one, and its W_s accordingly revised (C. H. Scholz & Contreras, 1998; Williams, Wedmore, Fagereng, et al., 2021a).

Source slip rates (S_s) are estimated using a systems-based approach that incorporates geodetically-derived regional extension rates (Wedmore et al., 2021; Williams, Mdala, et al., 2021; Williams, Wedmore, Fagereng, et al., 2021a), except for some sources in Lake Malawi, where slip rates can be derived from offsets across a 75 Ka reflector in seismic reflection surveys (Shillington et al., 2020). Slip rate estimates are then combined with $\bar{D}_s$ to derive an earthquake recurrence interval (R_s) estimate for each source through the relationship $R_s = \bar{D}_s / S_s$ (Wallace, 1970; Stirling et al., 2012).

4.2 The Adapted Approach to the Malawi Seismogenic Source Database

The discrete section, fault, and multifault sources in the MSSD are not an exhaustive list of potential earthquake ruptures in Malawi; in reality earthquakes can 'float' anywhere within a larger fault network (Visini et al., 2020; Field et al., 2021). In addition, Eq. 1 suggests that a source's down-dip extent is dependent on its length ('length-limited'), however, we cannot exclude the

possibility that, unless intersected by another source, all the MSSD sources propagate through Malawi's 35 km thick seismogenic layer ('layer-limited'). This uncertainty is raised further in Malawi by: (1) lateral variations in the lower crust's composition and strain rate that can locally modulate whether the down-dip extent of faults is seismic or aseismic (Fagereng, 2013; Hellebrekers et al., 2019; Wedmore, Biggs, et al., 2020), and (2) intrarift faults in Malawi may accommodate upper-crustal flexural extensional strains that are induced from bending in the hanging-wall of large displacement (>5 km) border faults (Turcotte & Schubert, 1982; Billings & Kattenhorn, 2005; Kolawole et al., 2018; Shillington et al., 2020).

We explore these uncertainties using an 'adapted' approach to the MSSD, which considers source area estimates (A_s) for both 'length-limited' and 'layer-limited' cases. We then combine A_s with source slip rates (S_s), and the regional b-value to develop continuous recurrence models that follow Gutenberg-Richter (G-R) or characteristic magnitude frequency distributions, and allow ruptures to float anywhere within the fault plane (Figs. 3 and 4; Youngs & Coppersmith, 1985; Convertito et al., 2006; Goda & Sharipov, 2021).

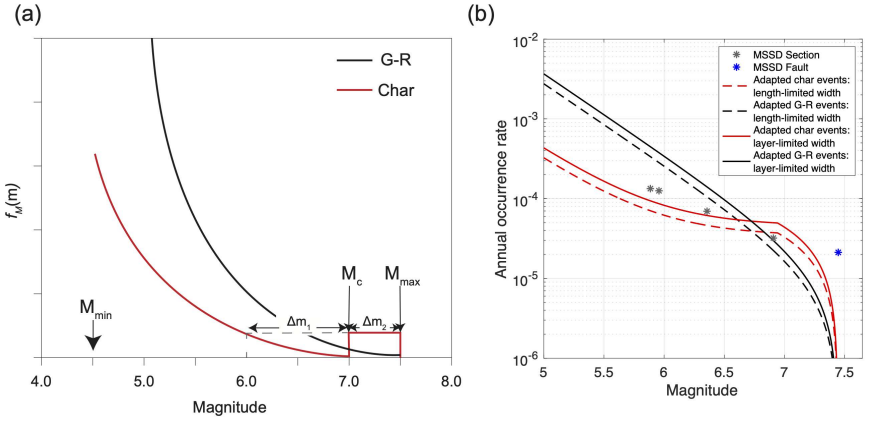

Fig. 3 (a) Schematic representation of the probability density functions for magnitude (m) for a continuous Gutenberg-Richter (G-R) and characteristic recurrence model (modified after Convertito et al., 2006). (b) Magnitude-frequency distribution curves for the Chingale Step Fault for the different cases of source width and recurrence models in the Adapted MSSD approach. Curves are for median b-value and M_{Max} estimates. Also shown are the discrete points in magnitude-frequency space for the Chingale Step fault source, and its constituent section sources in the Direct MSSD approach.

To apply this approach, we first calculate a source's seismic moment release rate ($\dot{M}_0$):

$$\dot{M}_0 = \mu S_s A_s \tag{2}$$

where μ is crustal rigidity and is taken as 33 GPa for consistency with the Leonard (2010) scaling relationships, and A_s is adjusted for length- and

layer-limited width cases. In distributing $\dot{M}_0$ across different magnitudes, the probability density function for magnitude m for a G-R recurrence model is given by:

$$f_M(m) = \frac{\beta e^{(-\beta(m-M_{min}))}}{1-e^{(-\beta(M_{Max}-M_{min}))}}, \text{ for } M_{min} \leq m \leq M_{Max} \tag{3}$$

where $\beta = b \ln 10$, and M_{min} and M_{Max} describe the range of event magnitudes that are assessed for each source. For a characteristic recurrence model, $f_M(m)$ is given by:

$$f_M(m) = \begin{cases} \frac{\beta e^{(-\beta(m-M_{min}))}}{(1+C)(1-e^{(-\beta(M_{Max}-M_{min}-\Delta m_2))})}, \text{ for } M_{min} \leq m \leq M_c \\ \\ \frac{\beta e^{(-\beta(M_{Max}-M_{min}-\Delta m_1-\Delta m_2))}}{(1+C)(1-e^{(-\beta(M_{Max}-M_{min}-\Delta m_2))})}, \text{ for } M_c \leq m \leq M_{Max} \end{cases} \tag{4}$$

where Δm_1 is the magnitude range across which the G-R portion of the source's magnitude-frequency relationship has a recurrence rate lower than the characteristic portion, Δm_2 is the magnitude range over which characteristic earthquakes occur, and which is bounded by the minimum characteristic earthquake magnitude (M_c) and M_{Max} (Fig. 3a; Youngs & Coppersmith, 1985; Convertito et al., 2006). The constant C is:

$$C = \frac{\beta e^{-(M_{Max}-M_{min}-\Delta m_1-\Delta m_2)}}{1-e^{(-\beta(M_{Max}-M_{min}-\Delta m_2))}} \Delta m_2 \tag{5}$$

The annual frequency, or 'activity rate,' for events with $m \geq M_{min}$ for a G-R magnitude frequency relationship (α_{GR}) is:

$$\alpha_{GR} = \frac{\dot{M}_0(c-b)(1-e^{(-\beta(M_{Max}-M_{min}))})}{bM_0^{Max}e^{-\beta(M_{Max}-M_{min})}} \tag{6}$$

where M_0^{Max} is the seismic moment for M_{Max}, and c is the parameter from the relation $\log M_0 = cm + d$ and equals 1.5 (Hanks & Kanamori, 1979). For characteristic earthquakes, the activity rate (α_C) is:

$$\alpha_C = \alpha_{NC} \frac{\beta \Delta m_2 e^{-\beta(M_{Max}-M_{min}-\Delta m_1-\Delta m_2)}}{1-e^{-\beta(M_{Max}-M_{min}-\Delta m_2)}} \tag{7}$$

where α_{NC} represents the activity rate of the non-characteristic magnitude range (i.e., for $M_{min} \leq m \leq M_c$, Fig. 3a), and is given by:

$$\alpha_{NC} = \frac{\dot{M}_0(1-e^{-\beta(M_{Max}-M_{min}-\Delta m_2)})}{KM_0^{Max}e^{-\beta(M_{Max}-M_{min}-\Delta m_2)}} \tag{8}$$

where the constant K is defined by:

$$K = \frac{b10^{-c\Delta m_2}}{c-b} + \frac{be^{\beta \Delta m_1}(1-10^{-c\Delta m_2})}{c} \tag{9}$$

To apply this approach to the MSSD, we use the regional b-value for Malawi (1.02; Poggi et al., 2017) and the Leonard (2010) area-magnitude scaling relationships to derive M_{Max}. Uncertainty in these parameters is explored by converting them to discrete variables, with the b-value shifted by $\pm$ 0.1 with weightings of 0.16 for lower and upper cases, and M_{Max} shifted $\pm$ 0.15 with weightings of 0.3 and 0.1 for lower and upper cases respectively (Fig. 2). Nine source-specific recurrence models can therefore be generated from sampling different combinations of these parameters, with these models more sensitive to variations in M_{Max} than the b-value (Fig. 20). M_{min} typically represents the smallest sized event of interest for hazard calculations and here equals 4.5. Following Youngs and Coppersmith (1985), Δm_1 and Δm_2 are 1.0 and 0.5 respectively. MSSD sources that are constituent parts of larger fault or multifault sources are implicitly incorporated into these continuous recurrence models, and so we do not consider these sources in the Adapted-MSSD approach.

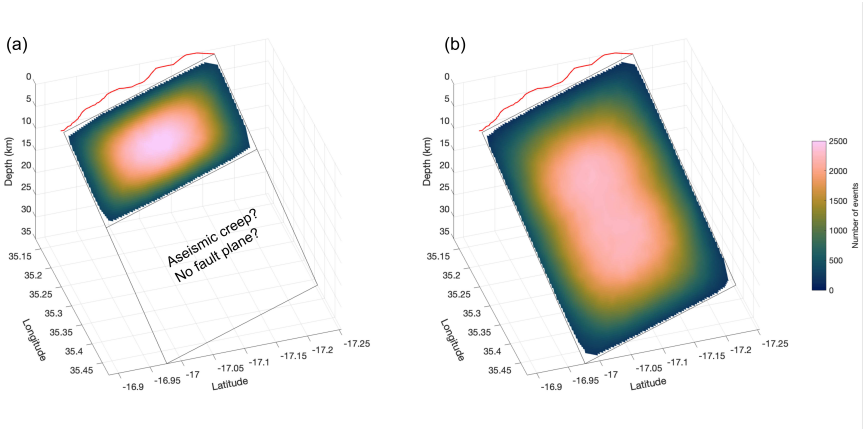

Fig. 4 Exploration of length-limited and layer-limited fault widths (W) in the Adapted MSSD approach for the Nsanje Fault source in the MSSD. In (a) W is assumed to be governed by its length through Eq. 1, with the fault planes either not propagating through the full-width of the seismogenic crust or the crust down-dip of the fault being aseismic. In (b) the fault plane is interpreted to extend through the 35 km thick seismogenic layer. The fault surface is then contoured by the distribution of events in the Adapted MSSD stochastic event catalogs. Red line depicts the Nsanje Fault's trace in the MAFD.

4.3 Areal sources

We use the areal source zones developed by Poggi et al. (2017) to incorporate: (1) earthquakes on unknown faults in Malawi, (2) earthquakes on faults included in the MAFD but not in the MSSD due to their short (<5 km) length (Williams, Wedmore, Fagereng, et al., 2021a), and (3) earthquakes in regions adjacent (< 200 km) to Malawi, where no fault-based earthquake sources have been developed (Fig. 5). These areal source zones are defined by a truncated

exponential G-R relationship where M_{min} is 4.5 (Table 2). Where areal sources are co-located within the region assessed for PSHA (Fig. 5), we limit M_{Max} from areal sources to 7.0, with the implicit assumption that all sources capable of a $M_W > 7.0$ earthquakes in this region are already included in the MSSD (Table 2).

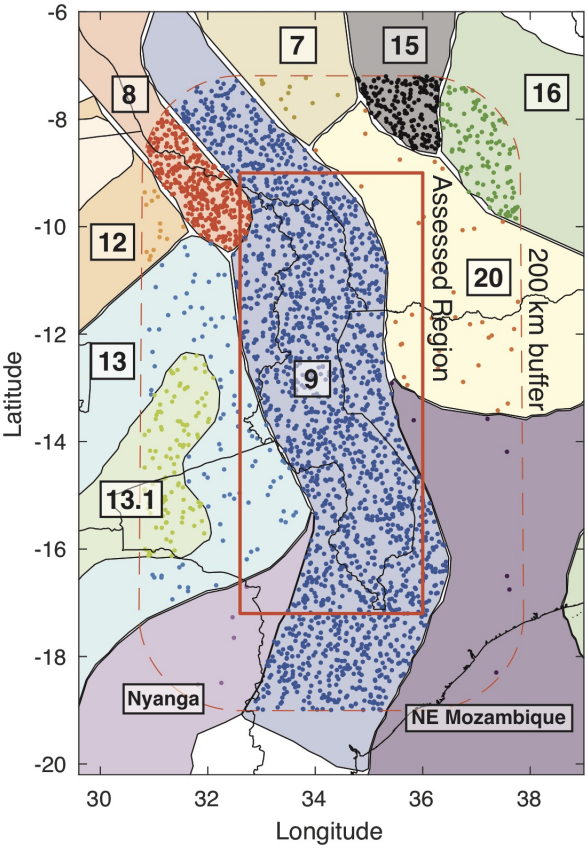

Fig. 5 Areal sources previously developed for PSHA in East Africa (Poggi et al., 2017). Numeric code for each zone corresponds to the Source ID in Table 2. Source zones (Nyanga and NE Mozambique) that are characterised by global stable craton seismicity (Fenton & Bommer, 2006) are also shown. Dots represent event locations from 1000 1-year long stochastic event catalogs for each source. In these catalogs, events are randomly located within each source and those >200 km from the assessed region are removed during the PSHA.

There are regions to the southwest and east of Malawi that are not covered by the Poggi et al. (2017) sources. However, since their seismic hazard is non-zero, we define areal sources for these regions by readjusting the a-value for

Table 2 Gutenberg-Richter and maximum magnitude (M_{Max}) parameters for areal source zones in Malawi and its surrounding (< 200 km) region

Source ID (Poggi et al., 2017)	Source Zone	*a*-value	*b*-value	M_{Max}
7	Lake Victoria	4	1.02	6.9
8	Tanganynika	4.84	1.02	7.9
9	Rukwa-Malawi	4.93	1.02	7.9[1]
12	Mweru South Katanga	4.05	0.99	6.9
13	Kariba-Okavango	4.08	0.99	6.9
13.1	Kariba-Okavango	3.99	0.99	6.9
15	Eastern Rift	5.31	1.17	7.4
16	Davie Rift	5.45	1.16	7.4
20	Rovuma Basin	3.31	1.02	6.9
N/A	Nyanga	1.73	0.8	7.0
N/A	Northeast Mozambique	1.93	0.8	7.0

Areal source zones taken from Poggi et al. (2017) or from adapting global rates of seismicity in stable cratons (Fenton et al., 2006). Extent of source zones shown in Fig. 5.

[1]M_{Max} revised to 7.0 for events occurring within Malawi during PSHA.

global stable craton seismicity to their respective areas (Fig. 5, Table 2; Fenton et al., 2006). Strictly speaking these regions do not meet the criteria of 'stable cratons' set by Fenton et al. (2006) as they are within 200 km of passive margins and/or regions of Phanerozoic deformation. However, given the lack of recorded earthquakes in these regions, these estimates remain the best constraint on their seismicity.

4.4 Stochastic Event Catalog Generation

To perform the PSHA, we generated five 2 million 1-year long simulations of MSSD- and areal source-based seismicity in Malawi. Each catalog combines an areal source catalog with a different interpretation of the MSSD: the Direct-MSSD approach (Section 4.1), and four catalogs developed from cumulatively exploring whether MSSD sources exhibit G-R or characteristic seismicity, and if their down-dip extrapolation is length- or layer-limited in the Adapted MSSD approach (Section 4.2, Figs. 2, 3, and 6). The identical length of each MSSD-based catalog is chosen to reflect that we have no constraints on what the 'true' fault width or magnitude-frequency distribution (MFD) is in Malawi, and so we equally weight each hypothesis (Frankel et al., 2000; Goda & Sharipov, 2021). Another interpretation is that these five catalogs can be merged into one 'Combined Catalog' that consists of 10 million 1-year catalog simulations (Fig. 6).

Earthquake occurrence is modelled in the catalogs using a memory-less Poisson process, and so for a given source, each event is independent of time (e.g., Zhuang et al., 2012; Pace et al., 2016). In the Direct-MSSD catalog, a source's annual occurrence rate (λ_s) is taken from the inverse of its recurrence interval, so that the time to its next event (t_s) is:

$$t_s = -\ln(1-u)/\lambda_s \tag{10}$$

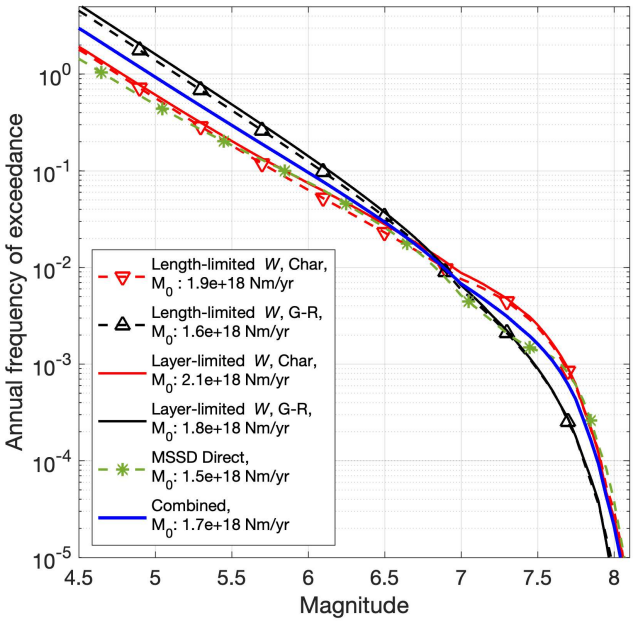

Fig. 6 Magnitude frequency distribution (MFD) and moment rate ($\dot{M}_0$) for the five simulated earthquake catalogs used in the PSHA. These catalogs are then merged into the 'Combined Catalog.' Note, this plot only considers areal source catalog events that occur within the assessed region shown in Fig. 5. G-R; Gutenberg-Richter

where u is a sample from the standard uniform distribution. The event magnitude is then sampled from a random normal variable centred around the source's Leonard (2010) magnitude-area scaling with a standard deviation of 0.1.

To derive weightings for section, fault, and multifault source events in the Direct-MSSD approach, we generated catalogs for all possible source type weighting combinations at intervals of 0.1 with the limitation that the weighting of any source type $\geq$ 0.1 (Fig. 7a). We then searched for the weighting combination that produced a MFD with the smallest Kolmogorov-Smirnov distance to a catalog with the regional b-value (1.02; Poggi et al., 2017) between M_W 6-7.6, across which the Direct-MSSD catalog is relatively complete (Fig. 7a). From this test, we find that weighting section, fault, and multifault sources by 0.6-0.3-0.1 respectively produces a catalog with a b-value closest to 1.02 (Fig. 7b). Alternative hypotheses must also be considered for where the MSSD sources splay in map view (Williams, Wedmore, Fagereng, et al., 2021a). In these cases, an equal weighting is applied for which branch will rupture.

Within each simulation cycle of the MSSD-Adapted catalogs, we randomly sample one of the nine recurrence models that is generated for each source width-MFD case (Fig. 20) given the weightings in Fig. 2. Then from the catalogs with a G-R MFD, λ_s equals α_{GR} as defined in Eq. 6, and event magnitudes

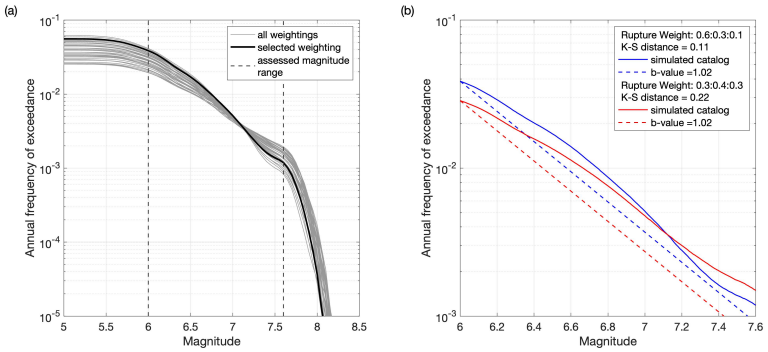

Fig. 7 (a) Magnitude frequency distributions (MFD) for the MSSD-Direct Catalog in which 36 possible weighting combinations of section, fault, and multifault ruptures are explored, with the MFD curve of the selected weighting combination highlighted. (b) MFD for the MSSD-Direct catalog with the optimal set of rupture weightings, defined by the smallest Kolomgorov-Smirnov (K-S) distance to the MFD of a catalog with a b-value of 1.02 (Poggi et al., 2017) over magnitudes M_W 6-7.6. For context, the same analysis for a case where each rupture has a relatively equal weighting is also shown.

are taken from the probability density function defined in Eq. 3. For a characteristic MFD, λ_s is defined by α_C (Eq. 7), and the magnitude of events is sampled from Eq. 4.

For the areal source catalog, λ_s and the magnitude distribution for each source is defined by its G-R relationship (Table 2). Events occur randomly anywhere within each source, however, events >200 km from the region assessed in the PSHA are subsequently removed (Fig. 5).

All events in the MSSD-based catalogs are presumed to be normal faulting earthquakes, which is consistent with their moderate fault dip, the regional stress state (Delvaux & Barth, 2010; Ebinger et al., 2019; Williams et al., 2019), Late Quaternary fault slickensides (Wedmore, Biggs, et al., 2020), and the offset of geological strata (Accardo et al., 2018; Shillington et al., 2020). However, of the 63 focal mechanisms that were resolved during a two year deployment of seismometers in northern Malawi, seven were strike-slip (Ebinger et al., 2019), and it has been proposed that some historical events elsewhere in the East Africa Rift were strike-slip (Ayele & Kulhanek, 2000). To recognise this 10% of events in the Areal Source Catalog are randomly assigned to be strike-slip.

4.5 Rupture Geometry

We define the rupture geometry of events in the MSSD-based catalogs using the MSSD geometric model (Fig. 8; Williams, Wedmore, Fagereng, et al., 2021a). This model consists of 2D planes in 3D space, however, for the purpose of source-to-site calculations, we convert it to a model defined by grid points at intervals of $1 \times 1 \times 0.6$ km in the $x \times y \times z$ direction respectively. The geometry

of each source in this model defines the lateral extent of events in the Direct-MSSD catalog. In addition, we allow the depth interval of smaller section or fault source to randomly float within a larger fault or multifault plane.

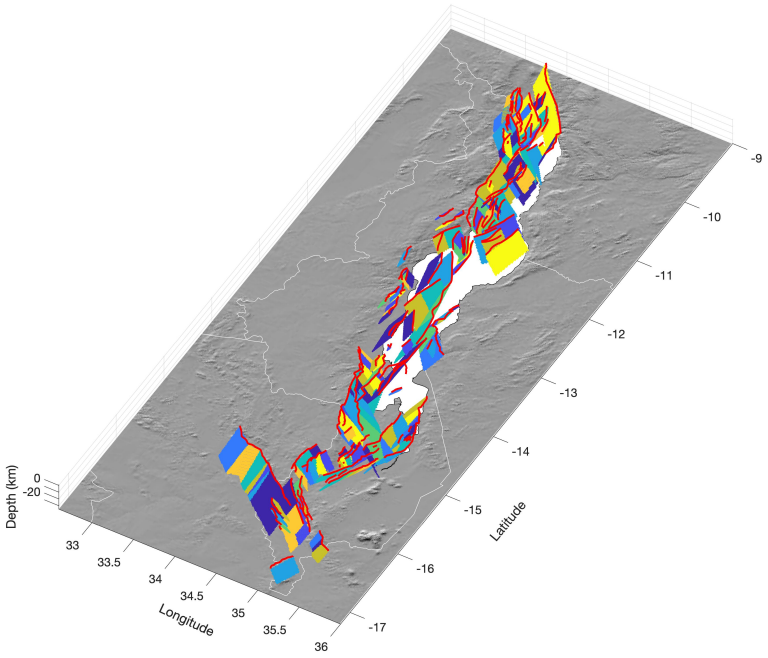

Fig. 8 3D model of MSSD sources used in the Direct MSSD and length-limited MSSD catalogs (Williams, Wedmore, Fagereng, et al., 2021a). The different colored planes represent either different MSSD fault sources, or multiple section sources along a single fault. Red lines are traces of the fault in the Malawi Active Fault Database. Image underlain by SRTM DEM

In the length-limited Adapted-MSSD catalogs, we use the same geometric source model as the Direct-MSSD catalog. However, in the layer-limited catalogs, we revise this model so that all sources are extrapolated to a depth of 35 km unless intersected by another source. The length and width of each event in the Adapted-MSSD catalogs are calculated from applying the inverse of the scaling relationships Leonard (2010) between source length, width and magnitude, and then floating this area randomly within the larger source plane (Fig. 4). In this approach, section boundaries or fault tips (for multi-fault sources) are not considered rupture barriers unlike in the Direct-MSSD Catalog.

In cases where MSSD sources intersect and it is not possible to fit a rupture onto the cut-off plane given Eq. 1, an area that matches the event's magnitude is randomly fitted onto the plane instead. To save computational resources, events M_W<5.4 in the Adapted-MSSD catalog are treated as point sources

and are randomly located on the source plane. Areal Source catalog events are also treated as point sources, and their depth is randomly sampled from a normal distribution with a mean of 20 km, standard deviation of 5 km, and that is truncated at 5 and 35 km.

4.6 Stochastic Event Catalog Validation

We test the output of the stochastic event catalogs in two ways: (1) internal tests to ensure consistency between the source's 'analytical' and catalog moment rate ($\dot{M}_0$), and (2) external tests to determine if the total $\dot{M}_0$ of these catalogs is consistent with independent constraints for the $\dot{M}_0$ in Malawi from instrumental seismicity (Poggi et al., 2017) and geodesy (Kreemer et al., 2014; Stamps et al., 2018).

For the Direct-MSSD internal tests, the analytical $\dot{M}_0$ of MSSD sources is calculated by combining the sources' magnitude and recurrence interval (R_s), with its source type weighting (Fig. 7), and for the Adapted-MSSD catalogs, through Eq. 2. Overall, we find there is a good correlation between these two $\dot{M}_0$ comparisons (Fig. 9) with the Direct-MSSD catalog and analytical total $\dot{M}_0$ equal to 1.17×10^{18} and 1.03×10^{18}Nm/yr respectively. The catalog for each areal source also indicates that it corresponds to its given G-R relation (Appendix A.1). These are important results because they indicate that the catalogs are representative of each source's seismicity, and hence can replace the need to numerically integrate over all possible values of source to site distance and magnitude as is performed in conventional PSHA (Musson, 1999; Atkinson & Goda, 2013).

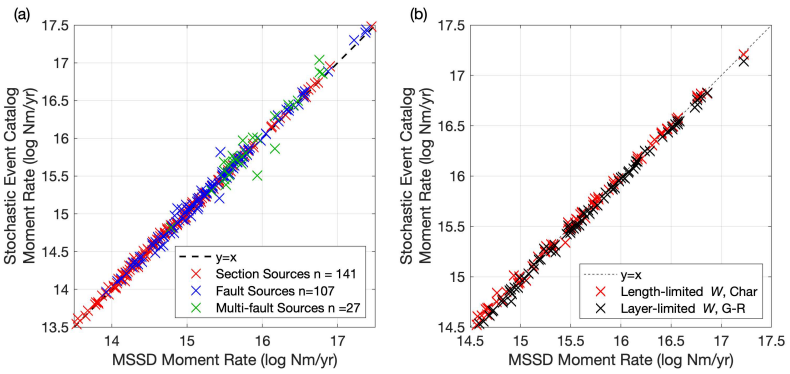

Fig. 9 Comparison of the analytical moment rate ($\dot{M}_0$) of sources in the MSSD and their $\dot{M}_0$ in (a) the Direct-MSSD catalog and (b) two of the Adapted-MSSD simulated catalogs.

The $\dot{M}_0$ of some multi-fault sources in the event catalogs does not match their analytical $\dot{M}_0$ (Fig. 9a). This reflects the long R_s and low (0.1) weighting

assigned to multifault sources in the Direct-MSSD catalog, which means there are insufficient simulation cycles to fully model their seismicity. We also find that for a given source width case, the total $\dot{M}_0$ of the characteristic catalog is higher than the G-R catalog (Fig. 6). This inconsistency with the $\dot{M}_0$ rate balancing approach results from the random variation of M_{Max} and selection of M_{min} when applying Eqs. 3-8. More simulation cycles would resolve these discrepancies, however, the additional computational costs are prohibitive.

For the external tests, we first estimate the $\dot{M}_0$ of the areal sources developed in Malawi by Poggi et al. (2017). This analysis considers their original M_{Max} estimate and so is representative of the $\dot{M}_0$ in Malawi from an extrapolated instrumental record (Appendix A.1). From this approach we derive a $\dot{M}_0$ of $\sim 7.5 \times 10^{17}$ Nm/yr (Table 3), which is less than ~50% of the $\dot{M}_0$ from the Combined Catalog ($\sim 1.7 \times 10^{18}$ Nm/yr, Fig. 6).

Part of this discrepancy reflects differences in the M_{Max} estimates for Malawi between Poggi et al. (2017) (7.9) and the MSSD-based Combined Catalog (8.1). If the MSSD-based M_{Max} estimate is applied to the areal source catalogs, their total $\dot{M}_0$ increases to 9.3 $\times 10^{17}$ Nm/yr. Thus, increasing M_{Max} reduces the $\dot{M}_0$ discrepancy, but cannot account for it alone. We therefore consider three other scenarios: (1) the geodetic $\dot{M}_0$ from which the slip-rates in the MSSD are mainly derived from (Wedmore et al., 2021) is released aseismically, (2) the geodetic $\dot{M}_0$ is an overestimate, or (3) extrapolating the instrumental record underestimates long-term earthquake activity in Malawi.

With regards to the first scenario, the nucleation of earthquakes throughout Malawi's seismogenic layer (Ebinger et al., 2019; Stevens et al., 2021), and energetic slowly decaying aftershock sequences implies overall highly coupled fault (Ben-Zion, 2008; Gaherty et al., 2019). However, some seismic moment may also be released by postseismic shallow afterslip (depths <5-10 km), as for example was observed following a M_W 5.2 earthquake near Karonga in 2014 (Zheng et al., 2020) and in the M_W 7.0 Machaze earthquake in Mozambique (Copley, Hollingsworth, & Bergman, 2012; Lloyd, Biggs, & Copley, 2019) .

For the second scenario, we compare the Combined Catalog to independent estimates of the geodetic $\dot{M}_0$ in Malawi from: (1) the Global Strain Rate Model (GSRM v.2.1; Kreemer et al., 2014) and (2) the Sub-Saharan African Geodetic Strain Rate Model (SSA-GSRM v.1.0; Stamps et al., 2018). Following the approach used in the seismic hazard inferred from tectonics (SHIFT) model (Bird & Liu, 2007; Bird & Kreemer, 2015), the $\dot{M}_0$ of the GSRM v2.1 and SSA-GSRM v1.0 models are 9.5×10^{17} Nm/yr and 3.5×10^{18} Nm/yr, respectively (Appendix A.2). The Combined Catalog $\dot{M}_0$ ($\sim 1.7 \times 10^{18}$ Nm/yr) is intermediate between these estimates. Furthermore, the MSSD slip rates that are derived from the 75 Ka. seismic reflector offsets in Lake Malawi are consistent with geodetically-derived regional extensional rates (Shillington et al., 2020; Wedmore et al., 2021; Williams, Wedmore, Fagereng, et al., 2021a).

The Combined Catalog $\dot{M}_0$ is also not necessarily identical to the input geodetic $\dot{M}_0$ since: (1) it incorporates events that accommodate hanging-wall flexural extension along intrarift faults in northern and central Malawi

(Williams, Wedmore, Fagereng, et al., 2021a), and this deformation will not be captured by large-scale geodetic models (Muirhead et al., 2016; Shillington et al., 2020), (2) areal source events are independent of the input geodetic $\dot{M}_0$, and (3) not all of the geodetic $\dot{M}_0$ is converted to seismic $\dot{M}_0$ due to the obliquity of MSSD sources to the regional extension direction (Williams, Mdala, et al., 2021) and/or because they do not extend across the full width of the seismogenic layer (Section 4.2 & Fig. 4). We calculate that if all MSSD sources were optimally oriented to the regional extension direction and extended to the base of the seismogenic layer, the total $\dot{M}_0$ would be 1.9×10^{18} Nm/yr (Appendix A.3). A physical interpretation of the difference between this $\dot{M}_0$ estimate and those from the event catalogs ($1.2 - 1.8 \times 10^{18}$ Nm/yr, Fig. 6) is that shallow aseismic deformation (Zheng et al., 2020) and off-fault events accommodate the deformation required to prevent space problems that would otherwise arise from normal fault obliquity and narrow fault widths in Malawi.

To investigate how likely it is that the observed seismicity in Malawi would have been simulated in our event catalogs, we divided the Combined Catalog into 50-year increments, and compared these samples $\dot{M}_0$ to the non-declustered 50 year long (1965-2015) SSA-GEM catalog (Poggi et al., 2017). We find an 11% chance that a 50 year sample of the Combined Catalog would have a $\dot{M}_0$ equal to or less than the SSA-GEM catalog $\dot{M}_0$ (Fig. 10a). Hence, if the Combined Catalog is representative of seismicity in Malawi, then the observed $\dot{M}_0$ between 1965-2015 is unusually, but not inconceivably, low.

We note too that there is <1% and <20% probability that the G-R and characteristic based catalogs $\dot{M}_0$ would be less than the SSA-GEM $\dot{M}_0$ (Fig. 10a). This result could be used to argue against applying G-R recurrence models to MSSD sources. However, the event catalogs are generated using a time-independent Poisson approach (Eq. 10), and it is plausible that clustered seismicity such as triggered events and/or long aftershock sequences, as occurred during the 2009 Karonga earthquakes, allow a MSSD source's MFD to align with a G-R relationship (Page & Felzer, 2015; Stirling & Gerstenberger, 2018; Wang et al., 2021). We suggest that if a non-Poission approach was used to generate the MSSD-catalogs (see Section 7.2), then more 50 year catalog samples would have a $\dot{M}_0$ that are comparable to the SSA-GEM catalog, even though the long-term deformation rates would not change.

In summary, there are many challenges in reconciling the Malawi's observed seismic $\dot{M}_0$ and the MSSD-Areal Combined $\dot{M}_0$. We propose that this reflects an incomplete instrumental earthquake record, which in turn is indicative of the limited duration, poor instrumental coverage, clustered seismicity, low regional extension rates, and locked faults (Ambraseys, 1991a; Biggs et al., 2010; Hodge et al., 2015; Stevens et al., 2021). This is further highlighted by the large uncertainty in how the catalog may be extrapolated to larger magnitudes (Fig. 10b; Tinti & Mulargia, 1987). Our analysis does not consider uncertainty within the MSSD itself, or with applying the Leonard (2010) scaling relationships to faults in Malawi. Nevertheless, the Combined Catalog does satisfy constraints on the distribution of across-rift regional extensional strain

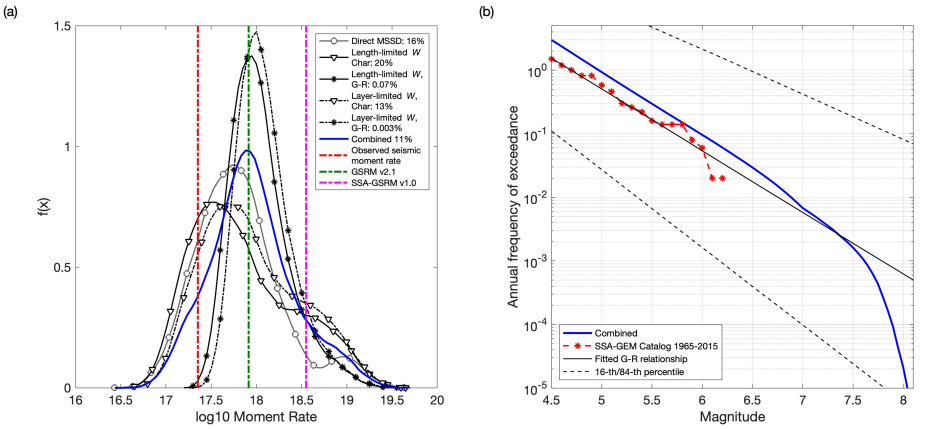

Fig. 10 (a) Comparison of the moment rate ($\dot{M}_0$) in 50 year samples of the stochastic event catalogs and the observed $\dot{M}_0$ from the SSA-GEM catalog between 1965-2015 for the assessed region shown in Fig. 5 (Poggi et al., 2017). Results for the Combined Catalog samples are shown as a kernel distribution (n=200,000) and are also resolved into the five different interpretations of the MSSD (n=40,000). The % by each catalog indicates the proportion of 50 year samples that had a $\dot{M}_0 \leq$ SSA-GEM catalog. For context, the $\dot{M}_0$ over the assessed region from the the Global Strain Model (GSRM v.2.1; Kreemer et al., 2014) and Sub-Saharan African Geodetic Strain Model (SSA-GSRM v.1.0; Stamps et al., 2018) are also shown (see also Appendix A). (b) Comparison of the Combined Catalog and SSA-GEM catalog magnitude-frequency distributions. We also fit and extrapolate a G-R relationship, and its associated uncertainties, to the SSA-GEM catalog for events M_W >4.5 following Tinti and Mulargia (1987). The SSA-GEM catalog has not been declustered in this analysis.

(Wedmore, Biggs, et al., 2020; Shillington et al., 2020), the regional b-value (Poggi et al., 2017), and the source specific $\dot{M}_0$ (Fig. 9). Furthermore, we have explored alternative hypotheses for uncertainty in on-fault magnitude-frequency distributions and fault down dip-extents. We therefore propose that it represents the best source model for PSHA currently available for Malawi.

5 Seismic hazard calculations

5.1 Ground motion model

In the absence of strong ground motion data in East Africa (Midzi et al., 1999; Hodge et al., 2015; Poggi et al., 2017), we apply ground motion models (GMMs) from other similar tectonic terranes. Specifically, there are variations between 1D seismic velocity models from northern and southern Malawi in the crust's top 5 km (Fig. 21; Ebinger et al., 2019; Stevens et al., 2021), which indicate GMMs from active and stable continental crust should be considered. In addition, large magnitude earthquakes in Malawi have generated remarkably little fracturing in the surrounding crust (Wedmore, Williams, et al., 2020). We therefore apply and equally weight three well-tested active crust GMMs (Chiou & Youngs, 2014; Akkar et al., 2014; Boore et al., 2014), and one stable

crust GMM (eastern crustal GMM from Atkinson & Adams, 2013). Some of these GMMs were previously applied in East Africa by Poggi et al. (2017), and the ratio of active to stable crust GMMs is equivalent to this study.

Cumulatively, these GMMs allow us to explore various source to site measurements: closest horizontal distance to rupture's surface projection (Joyner-Boore distance, R_{JB}), closest distance to rupture plane (R_{rup}), epicentral distance (R_{epi}), and hypocentral distance (R_{hypo}). In the instances that R_{epi} and R_{hypo} are applied to the MSSD fault-based events, distances are measured to a point randomly sampled within the simulated rupture's geometry. $R_{hypo} < 10$ km are not considered by the Atkinson and Adams (2013) GMM, in these instances, ground motions are calculated with R_{hypo} fixed to 10 km.

To incorporate aleatory uncertainty, the respective sigma model for each GMM is applied to the calculated median ground motion. For the site-specific PSHA in the three largest cities in Malawi (Lilongwe, Blantryre, and Mzuzu, Fig. 1), V_{S30} is set to reference values of 300 and 760 m/s and a range of spectral accelerations (SA) between 0-3 s are considered. For the PSHA maps, which are developed from 756 sites across Malawi in a $0.2° \times 0.2°$ latitude and longitude grid, we consider PGA only and both a reference V_{S30} value (760 m/s) and the site-specific value derived from the USGS V_{S30} database (Fig. 19; Wald & Allen, 2007).

5.2 Sensitivity analysis

We calculate the seismic hazard and its uncertainty by following the ensemble modelling framework used in the latest Italian seismic hazard model (Modello di Pericolosità Sismica (MPS19); Marzocchi et al., 2015; Meletti et al., 2021). In this approach, N seismic hazard curves are generated for each site, where N is the number of source model-GMM combinations. For a given PoE and SA, N hazard values can therefore be sampled and fitted to a continuous distribution (i.e., 'horizontal dissections' of the curves; Meletti et al., 2021), where the central value represents the seismic hazard estimate and the dispersion mimics the epistemic uncertainty (Marzocchi et al., 2015). In this study, N=20 given that we consider four GMMs and five interpretations of the MSSD in the stochastic event catalogs (Figs. 2 and 6). For each catalog-GMM combination, the annual probability (or rate) at which a specific ground motion intensity is exceeded ($v_{GM} \geq gm$) is calculated given the catalog's 2 million year length (Section 4.4).

For the site-specific PSHA, the 20 ground motion intensity values at a given PoE and SA are described by a beta distribution, as this provides good fits to unimodal distributions bounded between 0 and 1 (Marzocchi et al., 2015). The spatial distribution of seismic hazard uncertainty is of greater interest for the PSHA maps, and so is described by: (1) the interquartile range of the 20 seismic hazard values calculated at each site and (2) their Coefficient of Variation (CoV). The former describes the spatial distribution of the absolute uncertainty, whilst the latter is indicative of the uncertainty once normalised by the hazard level (Meletti et al., 2021). This analysis provides only

a minimum bound on hazard uncertainty as we do not consider the uncertainty in the MSSD slip rate and recurrence intervals estimates (Williams, Wedmore, Fagereng, et al., 2021a), the areal sources (Poggi et al., 2017), or the nine logic tree branches explored in the Adapted MSSD catalogs (Figs. 2 and 20). Stochastic event catalog generation and seismic hazard calculations were performed using bespoke codes written in MATLAB and available at https://github.com/jack-williams1/Malawi_PSHA.

6 PSHA Results

6.1 Site specific PSHA

The seismic hazard of the three selected sites (Lilongwe, Blantyre, and Mzuzu, Fig. 1) shows considerable diversity. The mean hazard is lowest in Lilongwe (10% PoE 0.11 g in 50 years for PGA and V_{S30} of 760 m/s), which is ∼55 km from the nearest MSSD source, and so local (<50 km) M_W 4-5 events in the areal source model present the main source of hazard (Figs. 11-13). The MSSD sources do, however, become important contributors to hazard in Lilongwe at low PoE and longer (>1 s) vibration periods (Fig. 12d). Hazard levels are higher in Blantyre and Mzuzu (10% PoE 0.15-0.2 g in 50 years). This reflects that both sites are < 20 km from MSSD sources, which dominate their hazard (Figs. 11-13).

Since the hazard at high PoE and short vibration periods is dominated by areal source events in Lilongwe, seismic hazard uncertainty is mainly driven by the ground motion model (GMM) selection (Fig. 11a). Conversely, in Blantyre and Mzuzu, both the source model (i.e., the event catalogs) and GMM selection contribute to uncertainty. In particular, high hazard levels are derived in Blantyre for the combinations that consider the Atkinson and Adams (2013) GMM and Gutenerg-Richter (G-R) on-fault frequency-magnitude distribution (MFD, Fig. 11e). However, in Mzuzu, the highest hazard levels are found for the Atkinson and Adams (2013) GMM regardless of the on-fault MFD (Fig. 11f). An important distinction between these sites that may explain this result, is the proximity of Mzuzu to the relatively high slip rate (>1 mm/yr) border faults around Lake Malawi (Fig. 1). Disaggregation analysis indicates that M_W 7-8 characteristic events along these faults are important contributors to seismic hazard in Mzuzu (Fig. 13c and f). In contrast, characteristic M_W 7-7.5 events along 50-100 km long, low slip-rate (0.1-1 mm/yr) sources around Blantyre are only important at low PoE (Fig. 13b). In all cases, the uncertainty in how the MSSD sources propagate through Malawi's 35 km thick seismogenic layer (i.e., length- or layer- limited width) do not significantly influence hazard estimates (Fig. 11).

6.2 Malawi Seismic Hazard Maps

We first assess the relative contribution of areal and MSSD sources to seismic hazard in Malawi through hazard maps that consider these sources separately.

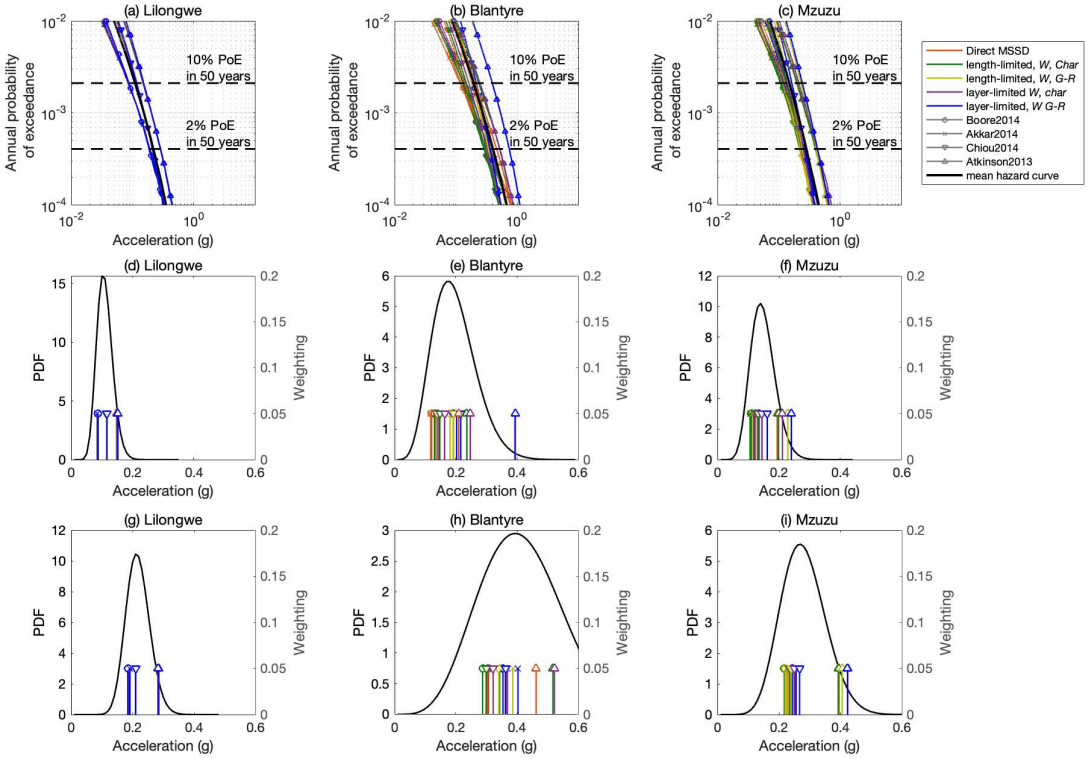

Fig. 11 (a)-(c) Seismic hazard curves for each assessed site and all event catalog-GMM combinations. The mean hazard curve generated from these different catalog-GMM combinations is also shown. Horizontal lines show the annual probabilities that are equivalent to 2% and 10% PoE in 50 years, and the hazard levels at these rates for all 20 event catalog-GMM combinations are shown in (d)-(e) and (f)-(h) respectively. In addition, we show the mean value and Beta distribution fitted to these values. Line colors represent different event catalogs, and symbols represent different GMMs. Analysis is for PGA and a V_{S30} condition of 760 m/s. An equivalent plot for 3 s spectral acceleration is shown in Fig. 22.

Figs. 15a and d indicates that the hazard from areal sources is generally spatially uniform, with a broad zone of relatively high hazard following the the relatively high $\dot{M}_0$ Rukwa-Malawi source zone (Tables 2 & 3, Figs. 5 & 17; Poggi et al., 2017), which broadly corresponds to the East African Rift's trajectory through Malawi (Fig. 1).

By contrast, the fault-based MSSD sources imply a more complex spatial pattern of seismic hazard, with localized regions of relatively high hazard (10% PoE ~0.2-0.3 g in 50 years) adjacent to rift-bounding 'border' faults in southern and northern Malawi (Fig. 14b & d). This reflects the relatively high slip rates assigned to border faults in the MSSD (~0.5-2 mm/yr Williams, Wedmore, Fagereng, et al., 2021a), which are based on Malawi's position within

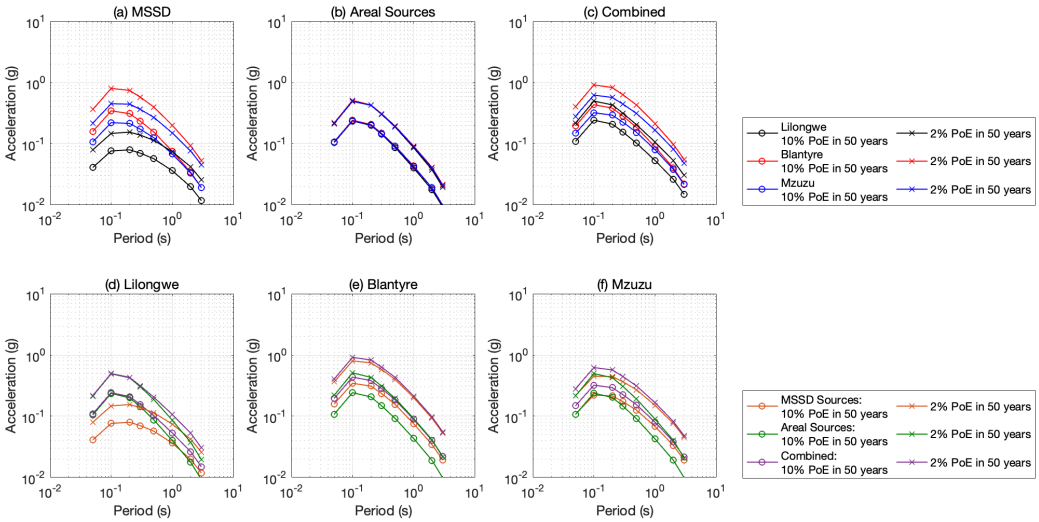

Fig. 12 Uniform hazard spectra for selected sites in Malawi for 2% and 10% PoE in 50 years, respectively and V_{S30}=760 m/s. (a-c) Hazard spectra sorted by source type. (d-f) Hazard spectra sorted by site.

an incipient amagmatic continental rift (Agostini et al., 2011; Accardo et al., 2018; Muirhead et al., 2019; Wright et al., 2020). In central Malawi, a greater proportion of the faults are under Lake Malawi, and so the MSSD sources have a less pronounced effect on the seismic hazard maps.

As observed in the site-specific PSHA, G-R recurrence models imply higher hazard levels than the Direct MSSD or characteristic approach (Fig. 15d & e). These differences are highest in southern Malawi (0.2 g for 10% PoE in 50 years), where MSSD slip rates are lower, and so relatively large magnitude Direct-MSSD or characteristic events are less likely to occur within the hazard timescale. The effect on hazard levels for different source down-dip extents are smaller (<0.1 g for 10% PoE in 50 years hazard levels) and localised to regions with relatively short (<50 km) MSSD sources (Fig. 15f). Cumulatively, these uncertainties mean that the spatial distribution of seismic hazard is highest adjacent to the MSSD sources (Fig. 15bc). This result is contrary to the Italian seismic hazard model where regions of high seismic hazard have low Coefficient of Variation (CoV) (Meletti et al., 2021). We note that peripheral areal sources also have relatively high CoV (Fig. 15c), but this likely reflects their low seismic hazard (Fig. 14) and not the underlying uncertainty in our analysis.

To quantify how the MSSD-Areal Combined map compares to seismic hazard maps previously developed for Malawi by Poggi et al. (2017) and Hodge et al. (2015), we find the closest sites within each map's respective grids, and then subtract the previous hazard estimates from the MSSD-Areal Combined value (Fig. 16). So that the differences we resolve in this comparison can be linked to the source model and GMMs alone, we consider only the MSSD generic

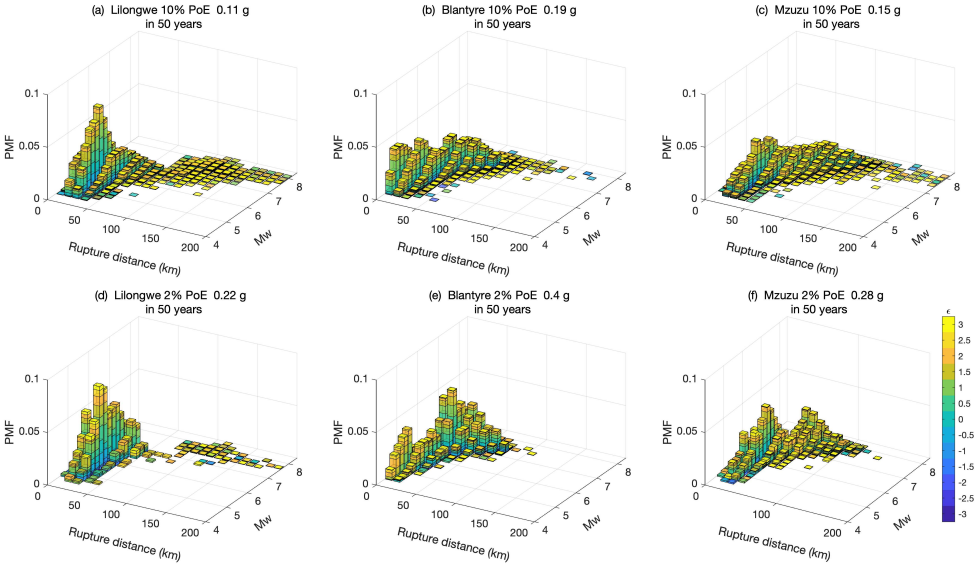

Fig. 13 Seismic disaggregation plots for PGA for Lilongwe, Blantyre and Mzuzu and (a-c) 10% and 2% (d-f) PoE in 50 years and V_{S30}=760 m/s.

near-surface rock condition values, (V_{S30} =760 m/s), and note this is higher than the equivalent value (V_{S30} =600 m/s) considered by Poggi et al. (2017).

For sites <40 km from the MSSD sources, our seismic hazard estimates for 10% PoE in 50 years level are up to 0.3 g higher than in the map from Poggi et al. (2017), with increases highest around the relatively high slip-rate border faults. The median difference between the Poggi et al. (2017) and MSSD-Areal combined maps is, however, only 0.015 g. This reflects that many sites in Malawi are far from active faults, and in these cases and at high PoE, areal sources are the main contributor to hazard. Indeed, at these sites, near-identical hazard levels are expected given that we incorporate off-fault seismicity using the areal sources from Poggi et al. (2017). Where they do exist, differences between these maps are likely a reflection of the selected GMMs and V_{S30} values.

For the 2% PoE in 50 years MSSD-Areal Combined map, hazard levels are generally higher than in Hodge et al. (2015), particularly at sites where new fault sources have been included (increases of 0.2-0.3 g). Locally, the MSSD-Areal combined map indicates lower hazard levels around the Bandawe and Mbamba faults (Fig. 16d). These faults were included as sources by Hodge et al. (2015) but not in the MSSD, as newer seismic reflection data indicates that these are inactive faults (McCartney & Scholz, 2016; Accardo et al., 2018; C. A. Scholz et al., 2020). Differences in GMM selection, and fault and areal source modelling may have also affected comparisons between these two maps, and we discuss this further in Section 7.1.

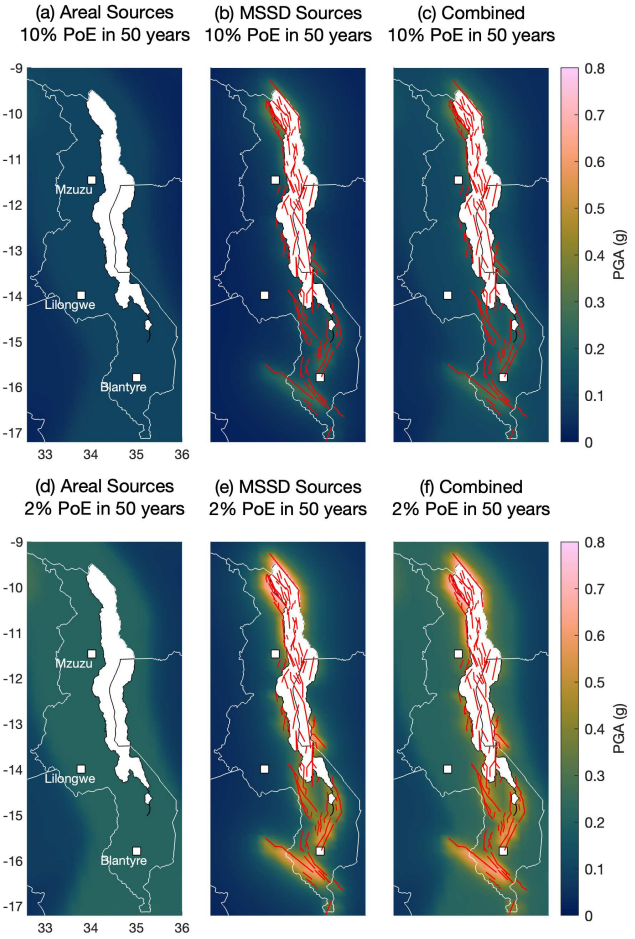

Fig. 14 Peak ground acceleration (PGA) seismic hazard maps for Malawi for (a)-(c) 10% PoE in 50 years, and (d)-(f) 2% PoE in 50 years for reference V_{S30} value (760 m/s). Figure is arranged so each column represents a different catalog. Red lines depict the MSSD sources (Williams, Wedmore, Fagereng, et al., 2021a). For equivalent maps for the slope-based USGS V_{S30} values (Wald & Allen, 2007), see Fig. 23.

7 Discussion

7.1 Seismic hazard and risk in Malawi

The moment rate ($\dot{M}_0$) implied by the MSSD-based catalogs leads to elevated seismic hazard estimates in Malawi compared to previous instrumental-seismicity based PSHA (Fig. 16; Poggi et al., 2017). However, this increase is only seen at sites $<\sim$40 km from the MSSD sources (Fig. 16a-c). This result

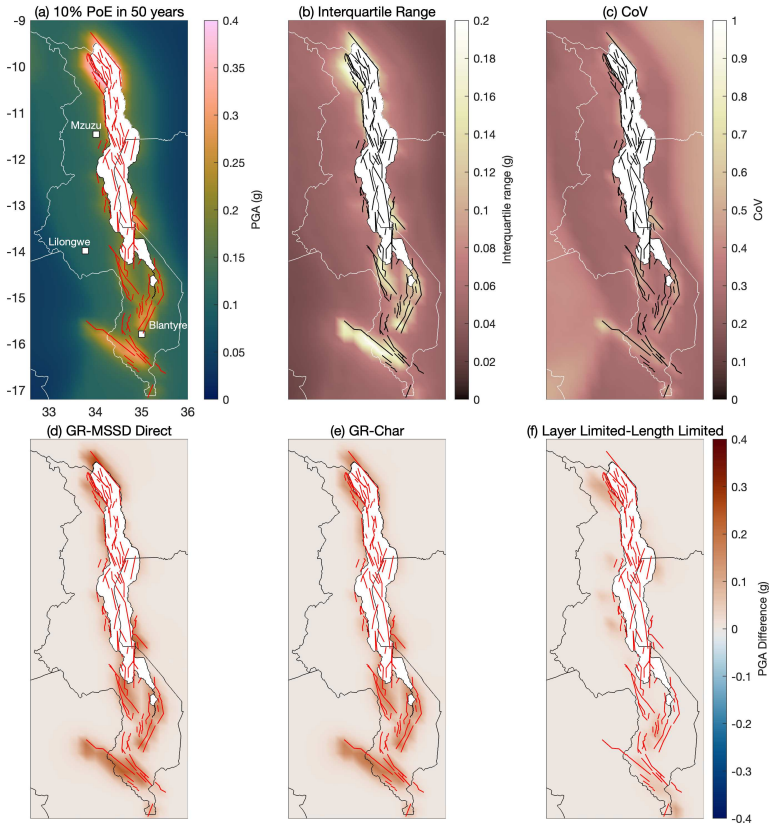

Fig. 15 Sensitivity analysis for seismic hazard maps. (a) Combined 10% PoE in 50 years seismic hazard map as shown in Fig. 14c, but with adjusted color axis. (b) Interquartile range of the 20 seismic hazard values calculated from each event catalog-GMM combination and (c) the Coefficient of Variation (CoV) of these values. (d)-(f) Maps showing how source modelling affects hazard uncertainty. (d) Difference in seismic hazard values for a Gutenberg-Richter (G-R) and MSSD Direct on-fault magnitude frequency distribution (MFD), for the length-limited case. (e) Same as (d) but comparison is between a G-R and characteristic MFD. (f) Difference in seismic hazard values for layer- and length-limited source down dip extents for a G-R on-fault MFD. All maps are for 10% PoE in 50 years hazard level, PGA, and the generic V_{S30} value (760 m/s). Comparison in (d)-(f) are for maps generated with the Boore et al. (2014) GMM.

demonstrates the importance of fault-based sources for understanding both the magnitude and spatial distribution of seismic hazard in Malawi.

Compared to the first generation of fault-based PSHA in Malawi (Hodge et al., 2015), the MSSD-Areal combined map indicates higher seismic hazard

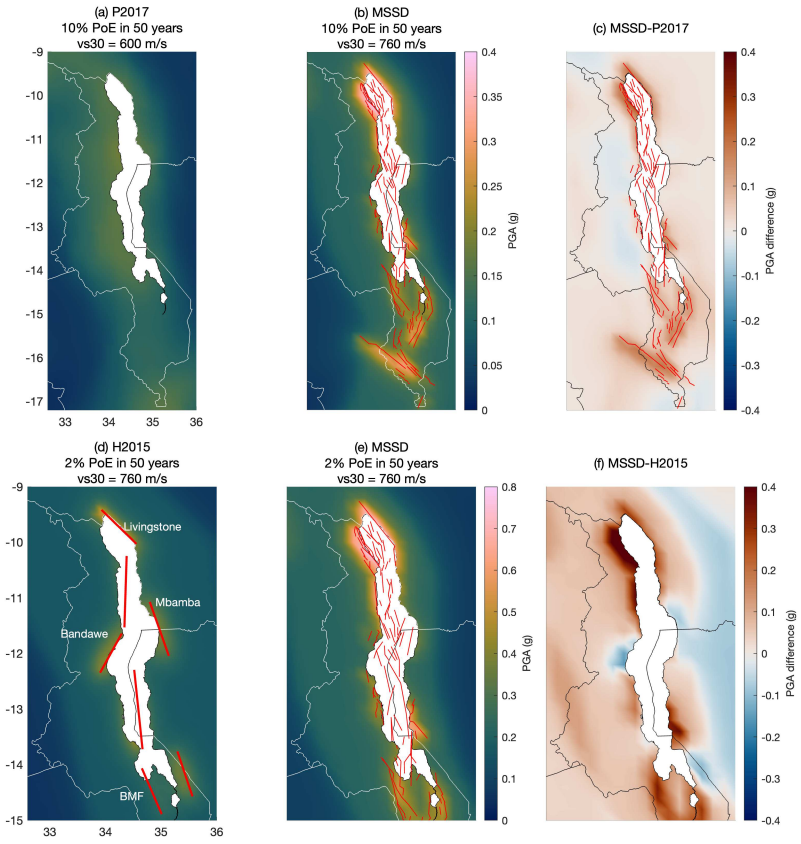

Fig. 16 (a-c) Comparison of peak ground acceleration (PGA) seismic hazard maps previously generated for Malawi by Poggi et al. (2017) and in this study for 10% PoE in 50 years respectively. (d-f) Equivalent to (a-c), but comparisons of our map with the mixed rupture catalog (MRC) 2% PoE in 50 years seismic hazard map for Malawi from Hodge et al. (2015). The MRC catalog represents an equal combination of segmented and continuous ruptures along fault sources in the Hodge et al. (2015) PSHA, except for the Livingstone and Bilila-Mtakataka (BMF) faults, which host continuous ruptures only. Red lines in (d) indicate fault sources used in Hodge et al. (2015). This map is truncated at 15°S, as fault sources south of Lake Malawi were not considered by Hodge et al. (2015).

levels in the East African Rift valley (Fig. 16d-f). This reflects the incorporation of new fault sources in the MSSD (107 vs 7), and in particular intrarift faults, which have been highlighted as overlooked seismic hazard sources in Malawi (Biggs et al., 2010; Shillington et al., 2020; Wedmore, Biggs, et al., 2020). However, the Livingstone Fault is broadly coincident between the two maps, and even though its slip rate estimate is lower in the MSSD (2.0 vs 3.8

mm/yr), the MSSD-Areal combined map implies higher seismic hazard adjacent to it (Fig. 16d-f). This reflects a combination of: (1) our exploration of on-fault Gutenberg-Richter (G-R) magnitude-frequency distribution (MFD), which leads to more frequent seismicity than the whole-fault events considered by Hodge et al. (2015), (2) our inclusion of a stable crust GMM, and our increased estimate for (3) the base of the seismogenic layer (35 vs 30 km), and (4) maximum background event magnitude (M_W 7 vs. M_W 6.25-6.75).

For global context, with a 10% PoE $\sim$ 0.2-0.3 g PGA in 50 years close to MSSD sources and 10% PoE $\sim$ 0.10-15 g PGA 50 years in regions peripheral to these sources (Fig. 14), the seismic hazard in Malawi can be considered comparable to other regions with low slip rate normal faults (Pagani et al., 2020), such as Italy (Meletti et al., 2021) and the Basin and Range Province in the USA (Petersen et al., 2015). Regional extension rates in Malawi are slightly lower than in these regions (0.5-1.5 mm/yr vs $\sim$3 mm/yr; D'Agostino et al., 2011; Hammond et al., 2014). However, this may be compensated for by the thicker seismogenic layer in Malawi, which implies its faults can attain great length scales, host larger magnitude earthquakes (Jackson & Blenkinsop, 1997), and so have a disproportionately high seismic M_0.

To fully explore and quantify the implications of this study for seismic risk in Malawi, results should be combined with seismic vulnerability and exposure assessments (Goda et al., 2016, 2021; Ngoma et al., 2019; Kloukinas et al., 2020; Giordano et al., 2021). Nevertheless, some implications of this PSHA to seismic risk are apparent. For example, given the low quality and high turnover of building stock in Malawi (Giordano et al., 2021), the results that are of most practical importance are for high PoE and in these instances the MSSD sources affect hazard levels only at long vibration periods and/or sites close ($<$ 40 km) to active faults (Fig. 12). Hence, off-fault areal sources are still important contributors to seismic risk in Malawi, and future work should consider improving its seismic network so that future PSHA can use a more finely resolved areal source model.

Instances where the hazard estimates at low PoE are of importance in Malawi are provided by railway bridges (Zant, 2018) and hydro-electric dams in the Shire River valley in southern Malawi, the latter of which generates 80% of Malawi's electricity (Taulo et al., 2015). The development of geothermal resources in Malawi, whose location are inherently controlled by active faults (Dulanya et al., 2010; Gondwe, 2015; Dávalos-Elizondo et al., 2021), should also consider local seismic hazard.

As with all PSHA of low strain rate regions, the ground motions derived at low PoE (typically 2% PoE in 50 years) do not necessarily represent an upper bound of what a site may experience (Reyners, 2011; Stein et al., 2012). This is demonstrated here by the Bilila-Mtakataka Fault, which locally may induce ground motions $\geq$ 0.8 g (Goda et al., 2021) compared to 0.3-0.5 g in our 2% PoE in 50 year PSHA maps (Fig. 14). Deterministic seismic hazard assessment may therefore be an important tool for investigating seismic risk in Malawi. Furthermore, PSHA only considers ground motions, and so other

possible secondary seismic hazards in Malawi, such as liquefaction, landslides and seiches (Williams, Wedmore, Scholz, et al., 2021a), are not considered here.

7.2 Using fault-based sources for PSHA in Malawi and other regions with a thick seismogenic layer and low strain rates

Fault-based MSSD sources are incorporated into PSHA in Malawi using stochastic event catalogs. Cumulatively these catalogs explore five different realisations of the MSSD (Fig. 2) in terms of the on-fault magnitude-frequency distribution (MFD) and the down-dip extension of faults through Malawi's seismogenic layer (i.e., 'length' or 'layer' limited faults). We consider alternative down-dip extents as it is not necessarily clear how sources should be extrapolated through Malawi's ∼35 km thick seismogenic layer (Eq. 1; e.g., Nyblade & Langston, 1995; Ebinger et al., 2019; Stevens et al., 2021). The influence of this uncertainty is only significant in regions in Malawi with relatively short (<50 km) sources (Fig. 15f). Longer sources are expected to extend throughout the seismogenic layer in either case under Eq. 1, and so the seismic hazard associated with these sources is not sensitive to their down-dip extrapolation.

Three on-fault MFD are considered for MSSD sources during the PSHA: G-R, characteristic, or the 'Direct-MSSD' approach where sources may rupture in geometrically defined sections, faults, or multifault ruptures (Fig. 3). We find that a G-R MFD generally implies higher hazard levels than a characteristic MFD (Figs. 11 and 15). This reflects that at the 100-1000's of years timescales that are of interest for seismic hazard assessment, the relatively frequent moderate magnitude (M_W 4.5-6.5, Fig. 6) events, which are inherent to a G-R MFD, are considerably more likely to occur in a low strain rate region than rare large magnitude characteristic events (Valentini et al., 2020; Goda & Sharipov, 2021). Although these differences reduce at lower PoE, they can still be significant for sites like Blantyre that are close to many long (> 50 km) low slip rate (0.05-1 mm/yr) faults. In the future, the on-fault MFD could be constrained in Malawi by inversion-based source models (Field et al., 2014, 2021; Chartier et al., 2019); however, a regional MFD target is required to apply these techniques, and it is not currently clear how this target should be defined for Malawi (Section 4.6).

Given that PSHA is sensitive to the assumed on-fault MFD, we consider it prudent that multiple cases should be explored in regions like Malawi with low strain rates and instrumental records much shorter than the earthquake recurrence intervals of individual faults. Although a smaller source of uncertainty, our results also imply that alternative cases could be considered for source down-dip extrapolation in regions with an abnormally thick seismogenic layer (>20 km) and short (<50 km) faults.

The stochastic event catalogs used in this PSHA are simulated using the assumption that earthquake inter-event times in Malawi follow a time-independent Poisson process (Section 4.4). However, the 2009 Karonga

earthquake sequence demonstrated that fault interaction through static stress changes can lead to clustered seismicity in Malawi (Biggs et al., 2010; Fagereng, 2013; Gaherty et al., 2019); indeed this is a widespread observation in low strain rate regions (e.g., Beanland & Berryman, 1989; Wedmore et al., 2017; Griffin et al., 2020). In these cases, earthquake interevent times are more appropriately modelled using two-parameter time-dependent distributions such as Weibull or Brownian Passage Time (Matthews et al., 2002; Zöller & Hainzl, 2007; Cowie et al., 2012). Seismic hazard assessment in Malawi should also recognise that previous large magnitude (M_W>7) earthquakes in the East African Rift were followed by long and damaging aftershock sequences (Ambraseys, 1991b, 1991a; Gaulon et al., 1992; Lloyd et al., 2019). It is, however, currently very difficult to incorporate these ideas into PSHA in Malawi as there is so little seismic or paleoseismic data. Future seismic hazard assessment in Malawi should consider these data when they become available.

7.3 Application of Ground Motion Models in Malawi

An ongoing challenge with PSHA in Malawi, and elsewhere in the East African Rift (EAR), is the lack of geotechnical (i.e., V_{S30} measurements) and strong motion data (GMMs; Midzi et al., 1999; Hodge et al., 2015; Poggi et al., 2017). This raises uncertainties when applying slope-based proxies for V_{S30} (Figs. 19 and 23), and means our use of global GMMs implicitly assumes that the ground motion behaviour in Malawi will be similar to other regions (i.e., the 'ergodic assumption;' Anderson & Brune, 1999). This could be addressed in future by considering whether regional weak ground motion data in Malawi can be used to adjust GMMs (Yenier & Atkinson, 2015). An additional problem is that EAR seismicity is characterised by deep moderate-large magnitude (M_W>6) normal fault earthquakes, and it is difficult to calibrate GMMs for these events as so few of them have been recorded (Boore et al., 2014; Akkar et al., 2014).

The incorporation of a stable crust GMM into PSHA in Malawi raises further challenges. In particular, the near-field (<10 km) motions associated with events in stable crust are poorly understood. This could be addressed though incorporation of the Next Generation Attenuation East (NGA-East) GMM (Goulet et al., 2018) in East Africa, and this would also allow R_{rup} to be considered in a stable crust GMMs. However, the NGA-East was developed for a reference V_{S30} condition of 3000 m/s, and challenges remain in adapting the site amplification factors for lower V_{S30} values (Kolaj et al., 2019) that are likely in Malawi (200-800 m/s, Fig. 19).

7.4 Implications for seismic hazard elsewhere in the East African Rift

Based on comparisons with previous instrumental catalog-based PSHA in Malawi (Fig. 16a-c), we highlight the limitations of using extrapolated instrumental catalogs to assess seismic hazard in regions with low strain rates and short catalog duration (Section 4.6). These challenges apply elsewhere in the

EAR, where despite abundant evidence for Late Quaternary faulting (e.g., Vittori et al., 1997; Lærdal & Talbot, 2002; Wanke, 2005; Kervyn et al., 2006; Zielke & Strecker, 2009; Fontijn et al., 2010; Nicholas et al., 2016; Delvaux et al., 2012, 2017; Muirhead et al., 2016; Daly et al., 2020; Siegburg et al., 2020), no fault-based PSHA has been attempted outside Malawi. This partly reflects the lack of chronostratigraphic data needed to estimate fault slip rates in the EAR, however, this can be addressed to an extent by incorporating regional geodetic data using the MSSD systems-based approach (Williams, Mdala, et al., 2021). Given the increasing levels of seismic risk (Goda et al., 2016; Meghraoui et al., 2016; Poggi et al., 2017; World-Bank, 2019), we suggest there is a clear need to develop new fault-based PSHA maps elsewhere in the EAR.

8 Conclusions

We use the Malawi Seismogenic Source Database (MSSD) to develop a new fault-based probabilistic seismic hazard analysis (PSHA) in Malawi. By including these sources, we show a more complex seismic hazard pattern in Malawi than previous instrumental-based PSHA (Poggi et al., 2017), with regions of elevated seismic hazard observed adjacent to relatively high slip rate rift-bounding faults. This replicates the findings of the 1st generation of fault-based PSHA in Malawi (Hodge et al., 2015). However, the incorporation of more fault sources in the MSSD (107 vs 7), source modelling, and ground motion model (GMM) selection, leads to a more complex seismic hazard pattern than Hodge et al. (2015). These results should motivate the development of more fault-based PSHA elsewhere in the EAR, as previous seismic hazard assessment has used the instrumental record of seismicity alone, and in some situations, this may underestimate hazard levels.

The stochastic event catalogs we use to incorporate the MSSD into PSHA explore alternative hypotheses for on-fault magnitude-frequency distribution (MFD) and the down-dip extension of fault-based sources through Malawi's 35 km thick seismogenic layer. We find that seismic hazard levels are only sensitive to the down-dip extension of relatively short sources (differences of $\sim$0.1 g for 10% PoE in 50 years for regions with $<$50 km long sources), whilst the assumed MFD can influence the hazard estimates for all sources. In particular, we find that compared to a characteristic MFD or 'direct' implementation of the MSSD, a Gutenberg-Richter MFD increases seismic hazard levels by up to 0.2 g for sites close to low slip rate sources ($<$1 mm /yr) and high PoE (10%PoE in 50 years).

Our new PSHA is also useful for highlighting sources of uncertainty, that present key targets for future research in Malawi. In particular, we highlight: (1) the uncertainty in fault slip rates, (2) the applicability of a Poisson model for earthquake recurrence, (3) refining off-fault areal sources, and (4) the lack of strong ground motion data. Nevertheless, we suggest our incorporation of a rich active fault and geodetic dataset makes this the most robust assessment

of seismic hazard currently available for Malawi, and presents a methodology for assessing seismic hazard also in other low strain rate regions.

Acknowledgments. This work was carried out using the computational facilities of the Advanced Computing Research Centre, University of Bristol - http://www.bris.ac.uk/acrc/. Color maps in Figs. 4, 23, 15, 16, 18, and 14 were produced following Crameri et al. (2020). We thank Vitor Silva (Global Earthquake Model Foundation) for providing us with the seismic hazard values from Poggi et al. (2017).

References

Accardo, N. J., Gaherty, J. B., Shillington, D. J., Hopper, E., Nyblade, A. A., Ebinger, C. J., ... Class, C. (2020). Thermochemical Modification of the Upper Mantle Beneath the Northern Malawi Rift Constrained From Shear Velocity Imaging. *Geochemistry, Geophysics, Geosystems*, *21*(6), 1–19. doi: 10.1029/2019GC008843

Accardo, N. J., Shillington, D. J., Gaherty, J. B., Scholz, C. A., Nyblade, A. A., Chindandali, P. R. N., ... Wambura Ferdinand, R. (2018). Constraints on Rift Basin Structure and Border Fault Growth in the Northern Malawi Rift From 3-D Seismic Refraction Imaging. *Journal of Geophysical Research: Solid Earth*, *123*(11), 3–10,10,25. doi: 10.1029/2018JB016504

Agostini, A., Bonini, M., Corti, G., Sani, F., & Mazzarini, F. (2011). Fault architecture in the Main Ethiopian Rift and comparison with experimental models: Implications for rift evolution and Nubia-Somalia kinematics. *Earth and Planetary Science Letters*, *301*(3-4), 479–492. doi: 10.1016/j.epsl.2010.11.024

Akkar, S., Sandıkkaya, M. A., & Bommer, J. J. (2014). Empirical ground-motion models for point- and extended-source crustal earthquake scenarios in Europe and the Middle East. *Bulletin of Earthquake Engineering*, *12*(1), 359–387. doi: 10.1007/s10518-013-9461-4

Ambraseys, N. N. (1991a). Earthquake hazard in the Kenya Rift: the Subukia earthquake 1928. *Geophysical Journal International*, *105*(1), 253–269. doi: 10.1111/j.1365-246X.1991.tb03460.x

Ambraseys, N. N. (1991b). The Rukuwa Earthquake of 13 December 1910 In East-Africa. *Terra Nova*, *3*(2), 202–211. doi: 10.1111/j.1365-3121.1991.tb00873.x

Anderson, J. G., & Brune, J. N. (1999). Probabilistic seismic hazard analysis without the ergodic assumption. *Seismological Research Letters*, *70*(1), 19–28. doi: 10.1785/gssrl.70.1.19

Atkinson, G. M., & Adams, J. (2013). Ground motion prediction equations for application to the 2015 Canadian national seismic hazard maps. *Canadian Journal of Civil Engineering*, *40*(10), 988–998.

Atkinson, G. M., & Goda, K. (2013). Probabilistic seismic hazard analysis of civil infrastructure. *Handbook of seismic risk analysis and management of civil infrastructure systems*, 3–28. doi: 10.1533/9780857098986.1.3

Ayele, A., & Kulhanek, O. (2000). *Reassessment of source parameters for three major earthquakes in the East African rift system from historical seismograms and bulletins* (Vol. 43) (No. 1). doi: 10.4401/ag-3627

Beanland, S., & Berryman, K. R. (1989). Style and episodicity of late quaternary activity on the pisa-grandview fault zone, Central Otago, New Zealand. *New Zealand Journal of Geology and Geophysics*, *32*(4), 451–461. doi: 10.1080/00288306.1989.10427553

Ben-Zion, Y. (2008). Collective behavior of earthquakes and faults: Continuum-discrete transitions, progressive evolutionary changes, and different dynamic regimes. *Reviews of Geophysics*, *46*(4), RG4006. doi:

10.1029/2008RG000260

Biggs, J., Nissen, E., Craig, T., Jackson, J., & Robinson, D. P. (2010). Breaking up the hanging wall of a rift-border fault: The 2009 Karonga earthquakes, Malawi. *Geophysical Research Letters*, *37*(11). doi: 10.1029/2010GL043179

Billings, S. E., & Kattenhorn, S. A. (2005). The great thickness debate: Ice shell thickness models for Europa and comparisons with estimates based on flexure at ridges. *Icarus*, *177*(2), 397–412. doi: 10.1016/j.icarus.2005.03.013

Bird, P., & Kreemer, C. (2015). Revised tectonic forecast of global shallow seismicity based on version 2.1 of the global strain rate map. *Bulletin of the Seismological Society of America*, *105*(1), 152–166. doi: 10.1785/0120140129

Bird, P., & Liu, Z. (2007). Seismic hazard inferred from tectonics: California. *Seismological Research Letters*, *78*(1), 37–48. doi: 10.1785/gssrl.78.1.37

Boore, D. M. (2016). Determining generic velocity and density models for crustal amplification calculations, with an update of the Boore and Joyner (1997) generic site amplification for Vs(Z) = m/s. *Bulletin of the Seismological Society of America*, *106*(1), 316–320. doi: 10.1785/0120150229

Boore, D. M., Stewart, J. P., Seyhan, E., & Atkinson, G. M. (2014). NGA-West2 equations for predicting PGA, PGV, and 5earthquakes. *Earthquake Spectra*, *30*(3), 1057–1085. doi: 10.1193/070113EQS184M

Bwambale, B., Bagampadde, U., Gidudu, A., & Martini, F. (2016). Seismic Hazard Analysis for the Albertine Region, Uganda – A Probabilistic Approach. *South African Journal of Geology*, *118*(4), 411–424. doi: 10.2113/gssajg.118.4.411

Chapola, L. S., & Kaphwiyo, C. E. (1992). The Malawi rift: Geology, tectonics and seismicity. *Tectonophysics*, *209*(1-4), 159–164. doi: 10.1016/0040-1951(92)90017-Z

Chartier, T., Scotti, O., & Lyon-Caen, H. (2019). Sherifs: Open-source code for computing earthquake rates in fault systems and constructing hazard models. *Seismological Research Letters*, *90*(4), 1678–1688. Retrieved from https://pubs.geoscienceworld.org/ssa/srl/article/570497/SHERIFS-OpenSource-Code-for-Computing-Earthquake doi: 10.1785/0220180332

Chiou, B. S. J., & Youngs, R. R. (2014). Update of the Chiou and Youngs NGA model for the average horizontal component of peak ground motion and response spectra. *Earthquake Spectra*, *30*(3), 1117–1153. doi: 10.1193/072813EQS219M

Chisenga, C., Dulanya, Z., & Jianguo, Y. (2019). The structural reinterpretation of the Lower Shire Basin in the Southern Malawi rift using gravity data. *Journal of African Earth Sciences*, *149*(September), 280–290. Retrieved from https://linkinghub.elsevier.com/retrieve/pii/S1464343X18302632 doi: 10.1016/j.jafrearsci.2018.08.013

Convertito, V., Emolo, A., & Zollo, A. (2006). Seismic-hazard assessment for a characteristic earthquake scenario: An integrated probabilistic-deterministic method. *Bulletin of the Seismological Society of America*, *96*(2), 377–391. doi: 10.1785/0120050024

Copley, A., Hollingsworth, J., & Bergman, E. (2012). Constraints on fault and lithosphere rheology from the coseismic slip and postseismic afterslip of the 2006 Mw7.0 Mozambique earthquake. *Journal of Geophysical Research: Solid Earth*, *117*(3). doi: 10.1029/2011JB008580

Cosentino, P., Ficarra, V., & Luzio, D. (1977). Truncated exponential frequency-magnitude relationship in earthquakes statistics. *Bulletin of the Seismological Society of America*, *67*(6), 1615–1623.

Cowie, P. A., Roberts, G. P., Bull, J. M., & Visini, F. (2012). Relationships between fault geometry, slip rate variability and earthquake recurrence in extensional settings. *Geophysical Journal International*, *189*(1), 143–160. doi: 10.1111/j.1365-246X.2012.05378.x

Cox, S. C., Stirling, M. W., Herman, F., Gerstenberger, M., & Ristau, J. (2012). Potentially active faults in the rapidly eroding landscape adjacent to the Alpine Fault, central Southern Alps, New Zealand. *Tectonics*, *31*(2). doi: 10.1029/2011TC003038

Craig, T. J., & Jackson, J. A. (2021). Variations in the Seismogenic Thickness of East Africa. *Journal of Geophysical Research: Solid Earth*, *126*(3), 1–15. doi: 10.1029/2020JB020754

Crameri, F., Shephard, G. E., & Heron, P. J. (2020). The misuse of colour in science communication. *Nature Communications*, *11*(1), 1–10. Retrieved from http://dx.doi.org/10.1038/s41467-020-19160-7 doi: 10.1038/s41467-020-19160-7

D'Agostino, N., Mantenuto, S., D'Anastasio, E., Giuliani, R., Mattone, M., Calcaterra, S., ... Bonci, L. (2011). Evidence for localized active extension in the central Apennines (Italy) from global positioning system observations. *Geology*, *39*(4), 291–294. doi: 10.1130/G31796.1

Daly, M. C., Green, P., Watts, A. B., Davies, O., Chibesakunda, F., & Walker, R. (2020). Tectonics and Landscape of the Central African Plateau and their Implications for a Propagating Southwestern Rift in Africa. *Geochemistry, Geophysics, Geosystems*, *21*(6). doi: 10.1029/2019GC008746

Dávalos-Elizondo, E., Atekwana, E. A., Atekwana, E. A., Tsokonombwe, G., & Laó-Dávila, D. A. (2021). Medium to low enthalpy geothermal reservoirs estimated from geothermometry and mixing models of hot springs along the Malawi Rift Zone. *Geothermics*, *89*. doi: 10.1016/j.geothermics.2020.101963

Delvaux, D., & Barth, A. (2010). African stress pattern from formal inversion of focal mechanism data. *Tectonophysics*, *482*(1-4), 105–128. doi: 10.1016/j.tecto.2009.05.009

Delvaux, D., Kervyn, F., Macheyeki, A. S., & Temu, E. B. (2012). Geodynamic significance of the TRM segment in the East African Rift (W-Tanzania):

Active tectonics and paleostress in the Ufipa plateau and Rukwa basin. *Journal of Structural Geology*, *37*, 161–180. doi: 10.1016/j.jsg.2012.01.008

Delvaux, D., Mulumba, J. L., Sebagenzi, M. N. S., Bondo, S. F., Kervyn, F., & Havenith, H. B. (2017). Seismic hazard assessment of the Kivu rift segment based on a new seismotectonic zonation model (western branch, East African Rift system). *Journal of African Earth Sciences*, *134*, 831–855. doi: 10.1016/j.jafrearsci.2016.10.004

Déverchère, J., Petit, C., Gileva, N., Radziminovitch, N., Melnikova, V., & San'Kov, V. (2001). Depth distribution of earthquakes in the Baikal rift system and its implications for the rheology of the lithosphere. *Geophysical Journal International*, *146*(3), 714–730.

Dixey, F. (1926). The Nyasaland section of the great rift valley. *The Geographical Journal*, *68*(2), 117–137.

Dulanya, Z. (2017). *A review of the geomorphotectonic evolution of the south Malawi rift* (Vol. 129). doi: 10.1016/j.jafrearsci.2017.02.016

Dulanya, Z., Morales-Simfors, N., & Sivertun, Å. (2010). Comparative study of the silica and cation geothermometry of the Malawi hot springs: Potential alternative energy source. *Journal of African Earth Sciences*, *57*(4), 321–327. doi: 10.1016/j.jafrearsci.2009.11.001

DuRoss, C. B., Personius, S. F., Crone, A. J., Olig, S. S., Hylland, M. D., Lund, W. R., & Schwartz, D. P. (2016). Fault segmentation: New concepts from the Wasatch Fault Zone, Utah, USA. *Journal of Geophysical Research: Solid Earth*, *121*(2), 1131–1157. doi: 10.1002/2015JB012519

Ebinger, C. J., Oliva, S. J., Pham, T. Q., Peterson, K., Chindandali, P., Illsley-Kemp, F., ... Mulibo, G. (2019). Kinematics of Active Deformation in the Malawi Rift and Rungwe Volcanic Province, Africa. *Geochemistry, Geophysics, Geosystems*, *20*(8), 3928–3951. doi: 10.1029/2019GC008354

Ebinger, C. J., Rosendahl, B. R., & Reynolds, D. J. (1987). Tectonic model of the Malaŵi rift, Africa. *Tectonophysics*, *141*(1-3), 215–235. doi: 10.1016/0040-1951(87)90187-9

Fagereng, Å. (2013). Fault segmentation, deep rift earthquakes and crustal rheology: Insights from the 2009 Karonga sequence and seismicity in the Rukwa-Malawi rift zone. *Tectonophysics*, *601*, 216–225. doi: 10.1016/j.tecto.2013.05.012

Fenton, C. H., Adams, J., & Halchuk, S. (2006). Seismic hazards assessment for radioactive waste disposal sites in regions of low seismic activity. *Geotechnical and Geological Engineering*, *24*(3), 579–592. doi: 10.1007/s10706-005-1148-4

Fenton, C. H., & Bommer, J. J. (2006, jul). The Mw7 Machaze, Mozambique, earthquake of 23 February 2006. *Seismological Research Letters*, *77*(4), 426–439. Retrieved from http://dx.doi.org/10.1785/gssrl.77.4.426 doi: 10.1785/gssrl.77.4.426

Field, E. H., Arrowsmith, R. J., Biasi, G. P., Bird, P., Dawson, T. E., Felzer,

K. R., ... Zeng, Y. (2014). Uniform California Earthquake Rupture Forecast, version 3 (UCERF3) -The time-independent model. *Bulletin of the Seismological Society of America*, *104*(3), 1122–1180. doi: 10.1785/0120130164

Field, E. H., Milner, K. R., & Page, M. T. (2021). Generalizing the inversion-based PSHA source model for an interconnected fault system. *Bulletin of the Seismological Society of America*, *111*(1), 371–390. doi: 10.1785/0120200219

Fontijn, K., Delvaux, D., Ernst, G. G. J., Kervyn, M., Mbede, E., & Jacobs, P. (2010). Tectonic control over active volcanism at a range of scales: Case of the Rungwe Volcanic Province, SW Tanzania; and hazard implications. *Journal of African Earth Sciences*, *58*(5), 764–777. Retrieved from http://dx.doi.org/10.1016/j.jafrearsci.2009.11.011 doi: 10.1016/j.jafrearsci.2009.11.011

Frankel, A. D., Mueller, C. S., Barnhard, T. P., Leyendecker, E. V., Wesson, R. L., Harmsen, S. C., ... Hanson, S. L. (2000). USGS national seismic hazard maps. *Earthquake spectra*, *16*(1), 1–19.

Fullgraf, T., Zammit, C., Bailly, L., Terrier, M., Hyvonen, E., Backman, B., ... Tychsen, J. (2017). *Geological Mapping and Mineral Assessment Project (GEMMAP) of Malawi. Report Inception Phase - February 2017.* (Tech. Rep.).

Gaherty, J. B., Zheng, W., Shillington, D. J., Pritchard, M. E., Henderson, S. T., Chindandali, P. R. N., ... Nettles, M. (2019). Faulting processes during early-stage rifting: Seismic and geodetic analysis of the 2009-2010 Northern Malawi earthquake sequence. *Geophysical Journal International*, *217*(3), 1767–1782. doi: 10.1093/gji/ggz119

Gaulon, R., Chorowicz, J., Vidal, G., Romanowicz, B., & Rouit, G. (1992). Regional geodynamic implications of the May-July 1990 earthquake sequence in southern Sudan. *Tectonophysics*, *209*(1-4), 87–103. doi: 10.1016/0040-1951(92)90012-U

Geist, E. L., & Parsons, T. (2018). Determining on-fault earthquake magnitude distributions from integer programming. *Computers and Geosciences*, *111*(November 2017), 244–259. Retrieved from https://doi.org/10.1016/j.cageo.2017.11.018 doi: 10.1016/j.cageo.2017.11.018

Giordano, N., De Risi, R., Voyagaki, E., Kloukinas, P., Novelli, V., Kafodya, I., ... Macdonald, J. (2021). Seismic fragility models for typical non-engineered URM residential buildings in Malawi. In *Structures* (Vol. 32, pp. 2266–2278). Elsevier. doi: 10.1016/j.istruc.2021.03.118

Goda, K., Gibson, E. D., Smith, H. R., Biggs, J., & Hodge, M. (2016). Seismic risk assessment of urban and rural settlements around lake malawi. *Frontiers in Built Environment*, *2*. Retrieved from http://journal.frontiersin.org/article/10.3389/fbuil.2016.00030/full doi: 10.3389/fbuil.2016.00030

Goda, K., Novelli, V., De Risi, R., Kloukinas, P., Giordano, N., Macdonald, J., ... Voyagaki, E. (2021). Scenario-based earthquake

risk assessment for central-southern Malawi: The case of the Bilila-Mtakataka Fault. *International Journal of Disaster Risk Reduction*, 102655. Retrieved from https://www.sciencedirect.com/science/article/pii/S2212420921006166 doi: https://doi.org/10.1016/j.ijdrr.2021.102655

Goda, K., & Sharipov, A. (2021). Fault-source-based probabilistic seismic hazard and risk analysis for victoria, british columbia, canada: A case of the leech river valley fault and devil's mountain fault system. *Sustainability*, *13*(3), 1–36. doi: 10.3390/su13031440

Goitom, B., Werner, M. J., Goda, K., Kendall, J. M., Hammond, J. O. S., Ogubazghi, G., ... Illsley-Kemp, F. (2017). Probabilistic seismic-hazard assessment for Eritrea. *Bulletin of the Seismological Society of America*, *107*(3), 1478–1494. doi: 10.1785/0120160210

Gómez-Novell, O., García-Mayordomo, J., Ortuño, M., Masana, E., & Chartier, T. (2020). Fault System-Based Probabilistic Seismic Hazard Assessment of a Moderate Seismicity Region: The Eastern Betics Shear Zone (SE Spain). *Frontiers in Earth Science*, *8*(December). doi: 10.3389/feart.2020.579398

Gondwe, K. T. (2015). Geothermal Energy Utilization Model for Nkhotakota Geothermal Springs in Malawi. no.

Goulet, C. A., Bozorgnia, Y., Abrahamson, N., Kuehn, N., Al Atik, L., Youngs, R., ... Atkinson, G. (2018). *Central and Eastern North America Ground-Motion Characterization - NGA-East Final Report* (No. 2018/08). Pacific Earthquake Engineering Research Center Berkeley, California.

Griffin, J. D., Stirling, M. W., & Wang, T. (2020). Periodicity and Clustering in the Long-Term Earthquake Record. *Geophysical Research Letters*, *47*(22), e2020GL089272. Retrieved from https://doi.org/10.1029/2020GL089272

Gupta, H. K., & Malomo, S. (1995). The Malawi earthquake of March 10, 1989: A report of the macroseismic survey. *Seismological Research Letters*, *66*(1), 20–27. doi: 10.1016/0040-1951(92)90018-2

Hamiel, Y., Baer, G., Kalindekafe, L., Dombola, K., & Chindandali, P. (2012). Seismic and aseismic slip evolution and deformation associated with the 2009-2010 northern Malawi earthquake swarm, East African Rift. *Geophysical Journal International*, *191*(3), 898–908. doi: 10.1111/j.1365-246X.2012.05673.x

Hammond, W. C., Blewitt, G., & Kreemer, C. (2014). Steady contemporary deformation of the central Basin and Range Province, western United States. *Journal of Geophysical Research: Solid Earth*, *119*, 5235–5253. doi: 10.1002/2014JB011145

Hanks, T. C., & Kanamori, H. (1979). A moment magnitude scale. In *Journal of geophysical research b: Solid earth* (Vol. 84, pp. 2348–2350). doi: 10.1029/JB084iB05p02348

Hellebrekers, N., Niemeijer, A. R., Fagereng, Å., Manda, B., & Mvula, R. L. S.

(2019). Lower crustal earthquakes in the East African Rift System: Insights from frictional properties of rock samples from the Malawi rift. *Tectonophysics*, *767*, 228167. doi: 10.1016/j.tecto.2019.228167

Helmstetter, A., & Werner, M. J. (2012). Adaptive spatiotemporal smoothing of seismicity for long-term earthquake forecasts in California. *Bulletin of the Seismological Society of America*, *102*(6), 2518–2529. doi: 10.1785/0120120062

Hodge, M., Biggs, J., Fagereng, A., Elliott, A., Mdala, H., & Mphepo, F. (2019). A semi-automated algorithm to quantify scarp morphology (SPARTA): Application to normal faults in southern Malawi. *Solid Earth*, *10*(1), 27–57. doi: 10.5194/se-10-27-2019

Hodge, M., Biggs, J., Fagereng, Å., Mdala, H., Wedmore, L., & Williams, J. (2020, feb). Evidence From High-Resolution Topography for Multiple Earthquakes on High Slip-to-Length Fault Scarps: The Bilila-Mtakataka Fault, Malawi. *Tectonics*, *39*(2), e2019TC005933. Retrieved from https://doi.org/10.1029/2019TC005933 doi: 10.1029/2019TC005933

Hodge, M., Biggs, J., Goda, K., & Aspinall, W. (2015). Assessing infrequent large earthquakes using geomorphology and geodesy: the Malawi Rift. *Natural Hazards*, *76*(3), 1781–1806. doi: 10.1007/s11069-014-1572-y

Holschneider, M., Zöller, G., & Hainzl, S. (2011). Estimation of the maximum possible magnitude in the framework of a doubly truncated Gutenberg-Richter model. *Bulletin of the Seismological Society of America*, *101*(4), 1649–1659. doi: 10.1785/0120100289

Hopper, E., Gaherty, J. B., Shillington, D. J., Accardo, N. J., Nyblade, A. A., Holtzman, B. K., ... Mbogoni, G. (2020). Preferential localized thinning of lithospheric mantle in the melt-poor Malawi Rift. *Nature Geoscience*, *13*(8), 584–589. doi: 10.1038/s41561-020-0609-y

Jackson, J., & Blenkinsop, T. (1993). The Malaŵi Earthquake of March 10, 1989: Deep faulting within the East African Rift System. *Tectonics*, *12*(5), 1131–1139. doi: 10.1029/93TC01064

Jackson, J., & Blenkinsop, T. (1997). The Bilila-Mtakataka fault in Malawi: an active, 100-km long, normal fault segment in thick seismogenic crust. *Tectonics*, *16*(1), 137–150. doi: 10.1029/96TC02494

Jackson, J., McKenzie, D., & Priestley, K. (2021). Relations between earthquake distributions, geological history, tectonics and rheology on the continents. *Philosophical Transactions of the Royal Society A: Mathematical, Physical and Engineering Sciences*, *379*(2193). doi: 10.1098/rsta.2019.0412

Kervyn, F., Ayub, S., Kajara, R., Kanza, E., & Temu, B. (2006). Evidence of recent faulting in the Rukwa rift (West Tanzania) based on radar interferometric DEMs. *Journal of African Earth Sciences*, *44*(2), 151–168. doi: 10.1016/j.jafrearsci.2005.10.008

Kloukinas, P., Novelli, V., Kafodya, I., Ngoma, I., Macdonald, J., & Goda, K. (2020). A building classification scheme of housing stock in Malawi for earthquake risk assessment. *Journal of Housing and the Built*

Environment, *35*(2), 507–537. doi: 10.1007/s10901-019-09697-5

Kolaj, M., Allen, T., Mayfield, R., Adams, J., & Halchuk, S. (2019). Ground-motion models for the 6 th Generation Seismic Hazard Model of Canada. *12th Canadian Conference on Earthquake Engineering*.

Kolawole, F., Atekwana, E. A., Laó-Dávila, D. A., Abdelsalam, M. G., Chindandali, P. R., Salima, J., & Kalindekafe, L. (2018). Active Deformation of Malawi Rift's North Basin Hinge Zone Modulated by Reactivation of Preexisting Precambrian Shear Zone Fabric. *Tectonics*, *37*(3), 683–704. Retrieved from http://dx.doi.org/10.1002/2017TC004628 doi: 10.1002/2017TC004628

Kolawole, F., Firkins, M. C., Al Wahaibi, T. S., Atekwana, E. A., & Soreghan, M. J. (2021). Rift interaction zones and the stages of rift linkage in active segmented continental rift systems. *Basin Research*. doi: 10.1111/bre.12592

Kreemer, C., Blewitt, G., & Klein, E. C. (2014). A geodetic plate motion and Global Strain Rate Model. *Geochemistry, Geophysics, Geosystems*, *15*(10), 3849–3889. doi: 10.1002/2014GC005407

Lærdal, T., & Talbot, M. R. (2002). Basin neotectonics of lakes Edward and George, East African Rift. *Palaeogeography, Palaeoclimatology, Palaeoecology*, *187*(3-4), 213–232. doi: 10.1016/S0031-0182(02)00478-9

Lavayssière, A., Drooff, C., Ebinger, C., Gallacher, R., Illsley-Kemp, F., Oliva, S. J., & Keir, D. (2019, feb). Depth Extent and Kinematics of Faulting in the Southern Tanganyika Rift, Africa. *Tectonics*, *38*(3), 842–862. Retrieved from https://doi.org/10.1029/2018TC005379 doi: 10.1029/2018TC005379

Leonard, M. (2010). Earthquake fault scaling: Self-consistent relating of rupture length, width, average displacement, and moment release. *Bulletin of the Seismological Society of America*, *100*(5 A), 1971–1988. doi: 10.1785/0120090189

Lloyd, R., Biggs, J., & Copley, A. (2019). The decade-long Machaze-Zinave aftershock sequence in the slowly straining Mozambique Rift. *Geophysical Journal International*, *217*(1), 504–531. doi: 10.1093/gji/ggz033

Macheyeki, A. S., Mdala, H., Chapola, L. S., Manhiça, V. J., Chisambi, J., Feitio, P., ... Tumwikirize, I. (2015). Active fault mapping in Karonga-Malawi after the December 19, 2009 Ms 6.2 seismic event. *Journal of African Earth Sciences*, *102*, 233–246. doi: 10.1016/j.jafrearsci.2014.10.010

Marzocchi, W., Taroni, M., & Selva, J. (2015). Accounting for epistemic uncertainty in PSHA: Logic tree and ensemble modeling. *Bulletin of the Seismological Society of America*, *105*(4), 2151–2159. doi: 10.1785/0120140131

Matthews, M. V., Ellsworth, W. L., & Reasenberg, P. A. (2002). A Brownian model for recurrent earthquakes. *Bulletin of the Seismological Society of America*, *92*(6), 2233–2250. doi: 10.1785/0120010267

McCartney, T., & Scholz, C. A. (2016). A 1.3 million year record of synchronous faulting in the hangingwall and border fault of a half-graben in the Malawi (Nyasa) Rift. *Journal of Structural Geology*, *91*, 114–129. doi: 10.1016/j.jsg.2016.08.012

Meghraoui, M., Amponsah, P., Ayadi, A., Ayele, A., Ateba, B., Bensuleman, A., ... Timoulali, Y. (2016). The seismotectonic map of Africa. *Episodes*, *39*(1), 9–18. doi: 10.18814/epiiugs/2016/v39i1/89232

Meletti, C., Marzocchi, W., D'Amico, V., Lanzano, G., Luzi, L., Martinelli, F., ... Visini, F. (2021). The new Italian seismic hazard model (MPS19). *Annals of Geophysics*, *64*(1), 1–29. doi: 10.4401/ag-8579

Midzi, V., Hlatywayo, D. J., Chapola, L. S., Kebede, F., Atakan, K., Lombe, D. K., ... Tugume, F. A. (1999). *Seismic hazard assessment in Eastern and Southern Africa* (Vol. V42) (No. No 6). doi: 10.4401/ag-3770

Msabi, M. M., & Ferdinand, R. W. (2021). Probabilistic seismic hazard analysis for Northern Tanzania Divergence Region and the adjoining areas. *Tanzania Journal of Science*, *47*(2), 862–876. doi: 10.4314/tjs.v47i2.40

Muirhead, J. D., Kattenhorn, S. A., Lee, H., Mana, S., Turrin, B. D., Fischer, T. P., ... Stamps, D. S. (2016). Evolution of upper crustal faulting assisted by magmatic volatile release during early-stage continental rift development in the East African Rift. *Geosphere*, *12*(6), 1670–1700. doi: 10.1130/GES01375.1

Muirhead, J. D., Wright, L. J. M., & Scholz, C. A. (2019). Rift evolution in regions of low magma input in East Africa. *Earth and Planetary Science Letters*, *506*, 332–346. doi: 10.1016/j.epsl.2018.11.004

Musson, R. M. W. (1999). Determination of design earthquakes in seismic hazard analysis through monte carlo simulation. *Journal of Earthquake Engineering*, *3*(4), 463–474. doi: 10.1080/13632469909350355

Ngoma, I., Kafodya, I., Kloukinas, P., Novelli, V., Macdonald, J., & Goda, K. (2019). Building classification and seismic vulnerability of current housing construction in Malawi. *Malawi Journal of Science and Technology*, *11*(1), 57–72.

Nicholas, C. J., Newth, I. R., Abeinomugisha, D., Tumushabe, W. M., & Twinomujuni, L. (2016). Geology and stratigraphy of the south-eastern Lake Edward basin (Petroleum Exploration Area 4B), Albertine Rift Valley, Uganda. *Journal of Maps*, *12*(2), 237–248.

Njinju, E. A., Kolawole, F., Atekwana, E. A. E. A., Stamps, D. S., Atekwana, E. A. E. A., Abdelsalam, M. G., & Mickus, K. L. (2019). Terrestrial heat flow in the Malawi Rifted Zone, East Africa: Implications for tectonothermal inheritance in continental rift basins. *Journal of Volcanology and Geothermal Research*, *387*. doi: 10.1016/j.jvolgeores.2019.07.023

Nyblade, A. A., & Langston, C. A. (1995). East African earthquakes below 20 km depth and their implications for crustal structure. *Geophysical Journal International*, *121*(1), 49–62. doi: 10.1111/j.1365-246X.1995.tb03510.x

Pace, B., Visini, F., & Peruzza, L. (2016). FiSH : MATLAB Tools to Turn

Fault Data into Seismic-Hazard Models. *Seismological Research Letters*, *87*(2A), 374–386. Retrieved from http://srl.geoscienceworld.org/lookup/doi/10.1785/0220150189 doi: 10.1785/0220150189

Pagani, M., Garcia-Pelaez, J., Gee, R., Johnson, K., Poggi, V., Silva, V., ... Weatherill, G. (2020). The 2018 version of the Global Earthquake Model: Hazard component. *Earthquake Spectra*, *36*(1), 226–251. doi: 10.1177/8755293020931866

Page, M., & Felzer, K. (2015). Southern San Andreas fault seismicity is consistent with the Gutenberg–Richter magnitude–frequency distribution. *Bulletin of the Seismological Society of America*, *105*(4), 2070–2080. doi: 10.1785/0120140340

Petersen, M. D., Moschetti, M. P., Powers, P. M., Mueller, C. S., Haller, K. M., Frankel, A. D., ... Olsen, A. H. (2015). The 2014 United States National Seismic Hazard Model. *Earthquake Spectra*, *31*, S1—-S30. doi: 10.1193/120814EQS210M

Philippon, M., Willingshofer, E., Sokoutis, D., Corti, G., Sani, F., Bonini, M., & Cloetingh, S. (2015). Slip re-orientation in oblique rifts. *Geology*, *43*(2), 147–150. doi: 10.1130/G36208.1

Poggi, V., Durrheim, R., Tuluka, G. M., Weatherill, G., Gee, R., Pagani, M., ... Delvaux, D. (2017). Assessing seismic hazard of the East African Rift: a pilot study from GEM and AfricaArray. *Bulletin of Earthquake Engineering*, *15*(11), 4499–4529. doi: 10.1007/s10518-017-0152-4

Reyners, M. (2011). Lessons from the destructive Mw 6.3 Christchurch, New Zealand, earthquake. *Seismological Research Letters*, *82*(3), 371–372. doi: 10.1785/gssrl.82.3.371

Saria, E., Calais, E., Stamps, D. S., Delvaux, D., & Hartnady, C. J. H. (2014). Present-day kinematics of the East African Rift. *Journal of Geophysical Research: Solid Earth*, *119*(4), 3584–3600. doi: 10.1002/2013JB010901

Scholz, C. A., Shillington, D. J., Wright, L. J. M., Accardo, N., Gaherty, J. B., & Chindandali, P. (2020). Intrarift fault fabric, segmentation, and basin evolution of the Lake Malawi (Nyasa) Rift, East Africa. *Geosphere*, *16*(5), 1293–1311. Retrieved from https://pubs.geoscienceworld.org/gsa/geosphere/article/588041/Intrarift-fault-fabric-segmentation-and-basin doi: 10.1130/GES02228.1

Scholz, C. H., Aviles, C. A., & Wesnousky, S. G. (1986). Scaling differences between large interplate and intraplate earthquakes. *Bulletin of the Seismological Society of America*, *76*(1), 65–70. Retrieved from http://www.bssaonline.org/content/76/1/65.short%5CnFile://localhost/Users/jescartin/WORK/Referencias/pdfs/Scholz1986.pdf doi: 10.1144/gsjgs.141.4.0763

Scholz, C. H., & Contreras, J. C. (1998). Mechanics of continental rift architecture. *Geology*, *26*(11), 967–970. doi: 10.1130/0091-7613(1998)026⟨0967:MOCRA⟩2.3.CO

Shillington, D. J., Gaherty, J. B., Ebinger, C. J., Scholz, C. A., Selway, K., Nyblade, A. A., ... Moshi, M. (2016). Acquisition of a unique

onshore/offshore geophysical and geochemical dataset in the northern Malawi (Nyasa) rift. *Seismological Research Letters*, *87*(6), 1406–1416. doi: 10.1785/0220160112

Shillington, D. J., Scholz, C. A., Chindandali, P. R. N., Gaherty, J. B., Accardo, N. J., Onyango, E., ... Nyblade, A. A. (2020). Controls on Rift Faulting in the North Basin of the Malawi (Nyasa) Rift, East Africa. *Tectonics*, *39*(3), e2019TC005633. doi: 10.1029/2019TC005633

Siegburg, M., Bull, J. M., Nixon, C. W., Keir, D., Gernon, T. M., Corti, G., ... Ayele, A. (2020). Quantitative Constraints on Faulting and Fault Slip Rates in the Northern Main Ethiopian Rift. *Tectonics*, *39*(8). doi: 10.1029/2019TC006046

Specht, T. D., & Rosendahl, B. R. (1989). Architecture of the Lake Malawi Rift, East Africa. *Journal of African Earth Sciences*, *8*(2-4), 355–382. doi: 10.1016/S0899-5362(89)80032-6

Stamps, D. S., Calais, E., Saria, E., Hartnady, C., Nocquet, J. M., Ebinger, C. J., & Fernandes, R. M. (2008). A kinematic model for the East African Rift. *Geophysical Research Letters*, *35*(5). doi: 10.1029/2007GL032781

Stamps, D. S., Kreemer, C., Fernandes, R., Rajaonarison, T. A., & Rambolamanana, G. (2021). Redefining East African Rift System kinematics. *Geology*, *49*(2), 150–155. doi: 10.1130/G47985.1

Stamps, D. S., Saria, E., & Kreemer, C. (2018). A Geodetic Strain Rate Model for the East African Rift System. *Scientific Reports*, *8*(1). doi: 10.1038/s41598-017-19097-w

Stein, S., Geller, R. J., & Liu, M. (2012). Why earthquake hazard maps often fail and what to do about it. *Tectonophysics*, *562-563*, 1–25. doi: 10.1016/j.tecto.2012.06.047

Stevens, V. L., Sloan, R. A., Chindandali, P. R., Wedmore, L. N. J., Salomon, G. W., & Muir, R. A. (2021). The Entire Crust can be Seismogenic: Evidence from Southern Malawi. *Tectonics*, *40*(6), e2020TC006654. doi: 10.1029/2020tc006654

Stirling, M., & Gerstenberger, M. (2018). Applicability of the Gutenberg-Richter relation for major active faults in New Zealand. *Bulletin of the Seismological Society of America*, *108*(2), 718–728. doi: 10.1785/0120160257

Stirling, M., McVerry, G., Gerstenberger, M., Litchfield, N., Van Dissen, R., Berryman, K., ... Jacobs, K. (2012). National seismic hazard model for New Zealand: 2010 update. *Bulletin of the Seismological Society of America*, *102*(4), 1514–1542. doi: 10.1785/0120110170

Taulo, J. L., Gondwe, K. J., & Sebitosi, A. B. (2015). Energy supply in Malawi: Options and issues. *Journal of energy in Southern Africa*, *26*(2), 19–32.

Tinti, S., & Mulargia, F. (1987). Confidence intervals of b values for grouped magnitudes. *Bulletin of the Seismological Society of America*, *77*(6), 2125–2134. Retrieved from http://www.bssaonline.org/content/77/6/2125.abstract

Tuluka, G. M., Lukindula, J., & Durrheim, R. J. (2020). Seismic Hazard

Assessment of the Democratic Republic of Congo and Environs Based on the GEM–SSA Catalogue and a New Seismic Source Model. *Pure and Applied Geophysics*, *177*(1), 195–214. doi: 10.1007/s00024-018-2084-6

Turcotte, D. L., & Schubert, G. (1982). *Geodynamics: Applications of continuum physics to geological problems, 450 pp.* John Wiley, New York.

Twiss, R. J., & Unruh, J. R. (1998). Analysis of fault slip inversions: Do they constrain stress or strain rate? *Journal of Geophysical Research: Solid Earth*, *103*(B6), 12205–12222. doi: 10.1029/98jb00612

Valentini, A., DuRoss, C. B., Field, E. H., Gold, R. D., Briggs, R. W., Visini, F., & Pace, B. (2020). Relaxing Segmentation on the Wasatch Fault Zone: Impact on Seismic Hazard. *Bulletin of the Seismological Society of America*, *110*(1), 83–109. doi: 10.1785/0120190088

Vallage, A., & Bollinger, L. (2020). Testing Fault Models in Intraplate Settings: A Potential for Challenging the Seismic Hazard Assessment Inputs and Hypothesis? *Pure and Applied Geophysics*, *177*(5), 1879–1889. doi: 10.1007/s00024-019-02129-z

Visini, F., Valentini, A., Chartier, T., Scotti, O., & Pace, B. (2020). Computational Tools for Relaxing the Fault Segmentation in Probabilistic Seismic Hazard Modelling in Complex Fault Systems. *Pure and Applied Geophysics*, *177*(5), 1855–1877. doi: 10.1007/s00024-019-02114-6

Vittori, E., Delvaux, D., & Kervyn, F. (1997). Kanda fault: A major seismogenic element west of the Rukwa Rift (Tanzania, East Africa). *Journal of Geodynamics*, *24*(1-4), 139–153. doi: 10.1016/S0264-3707(96)00038-5

Wald, D. J., & Allen, T. I. (2007). Topographic slope as a proxy for seismic site conditions and amplification. *Bulletin of the Seismological Society of America*, *97*(5), 1379–1395. doi: 10.1785/0120060267

Wallace, R. E. (1970). Earthquake recurrence intervals on the San Andreas fault. *Bulletin of the Geological Society of America*, *81*(10), 2875–2890. doi: 10.1130/0016-7606(1970)81[2875:ERIOTS]2.0.CO;2

Wang, S., Werner, M. J., & Yu, R. (2021). How Well Does Poissonian Probabilistic Seismic Hazard Assessment (PSHA) Approximate the Simulated Hazard of Epidemic-Type Earthquake Sequences? *Bulletin of the Seismological Society of America*, 1–19. doi: 10.1785/0120210022

Wanke, H. (2005). The namibian Eiseb Graben as an extension of the east African Rift: Evidence from Landsat TM 5 imagery. *South African Journal of Geology*, *108*(4), 541–546. doi: 10.2113/108.4.541

Wedmore, L., Biggs, J., Floyd, M., Fagereng, Mdala, H., Chindandali, P., ... Mphepo, F. (2021). Geodetic Constraints on Cratonic Microplates and Broad Strain During Rifting of Thick Southern African Lithosphere. *Geophysical Research Letters*, *48*(17). doi: 10.1029/2021GL093785

Wedmore, L., Biggs, J., Williams, J., Fagereng, Å., Dulanya, Z., Mphepo, F., & Mdala, H. (2020, feb). Active Fault Scarps in Southern Malawi and Their Implications for the Distribution of Strain in Incipient Continental Rifts. *Tectonics*, *39*(3), e2019TC005834. Retrieved from https://doi.org/10.1029/2019TC005834 doi: 10.1029/2019TC005834

Wedmore, L., Faure Walker, J. P., Roberts, G. P., Sammonds, P. R., McCaffrey, K. J. W., & Cowie, P. A. (2017). A 667 year record of coseismic and interseismic Coulomb stress changes in central Italy reveals the role of fault interaction in controlling irregular earthquake recurrence intervals. *Journal of Geophysical Research: Solid Earth*, *122*(7), 5691–5711. doi: 10.1002/2017JB014054

Wedmore, L., Williams, J., Biggs, J., Fagereng, Å., Mphepo, F., Dulanya, Z., ... Adams, B. A. (2020). Structural inheritance and border fault reactivation during active early-stage rifting along the Thyolo fault, Malawi. *Journal of Structural Geology*, *139*, 104097. doi: 10.1016/j.jsg.2020.104097

Williams, J., Fagereng, Å., Wedmore, L., Biggs, J., Mphepo, F., Dulanya, Z., ... Blenkinsop, T. (2019). How Do Variably Striking Faults Reactivate During Rifting? Insights From Southern Malawi. *Geochemistry, Geophysics, Geosystems*, *20*(7), 3588–3607. doi: 10.1029/2019GC008219

Williams, J., Mdala, H., Fagereng, Å., Wedmore, L., Biggs, J., Dulanya, Z., ... Mphepo, F. (2021). A systems-based approach to parameterise seismic hazard in regions with little historical or instrumental seismicity: Active fault and seismogenic source databases for southern Malawi. *Solid Earth*, *12*(1), 187–217. doi: 10.5194/se-12-187-2021

Williams, J., Wedmore, L., Fagereng, Å., Werner, M., Mdala, H., Shillington, D., ... Chindandali, P. (2021a). Geologic and geodetic constraints on the seismic hazard of Malawi's active faults : The Malawi Seismogenic Source Database (MSSD). *Natural Hazards and Earth System Science*(November). doi: https://doi.org/10.5194/nhess-2021-306

Williams, J., Wedmore, L., Fagereng, Å., Werner, M., Mdala, H., Shillington, D., ... Chindandali, P. (2021b, oct). Malawi Seismogenic Source Database (v1.0) [Data set]. Retrieved from https://zenodo.org/record/5599617#.YgbBHS8RpQY doi: 10.5281/ZENODO.5599617

Williams, J., Wedmore, L., Scholz, C., Kolawole, F., Wright, L., Shillington, D., ... Werner, M. J. (2021b, sep). Malawi Active Fault Database (v1.0) [Data set]. Retrieved from https://zenodo.org/record/5507190#.YgbBiy8RpQZ doi: 10.5281/ZENODO.5507190

Williams, J., Wedmore, L., Scholz, C. A., Kolawole, F., Wright, L., Shillington, D., ... Werner, M. (2021a). The Malawi Active Fault Database: an onshore-offshore database for regional assessment of seismic hazard and tectonic evolution. *Earth and Space Science Open Archive ESSOAr*.

World-Bank. (2019). *Tectonic Shift : Rift 2018 - Regional Seismic Risk and Resilience Workshop (English)* (Tech. Rep.). Washington, D.C. : World Bank Group. Retrieved from http://documents.worldbank.org/curated/en/325121555063464245/Tectonic-Shift-Rift-2018-Regional-Seismic-Risk-and-Resilience-Workshop

Wright, L. J. M., Muirhead, J. D., & Scholz, C. A. (2020). Spatiotemporal Variations in Upper Crustal Extension Across the Different Basement

Terranes of the Lake Tanganyika Rift, East Africa. *Tectonics*, *39*(3). doi: 10.1029/2019TC006019

Yenier, E., & Atkinson, G. M. (2015). Regionally adjustable generic ground-motion prediction equation based on equivalent point-source simulations: Application to central and eastern North America. *Bulletin of the Seismological Society of America*, *105*(4), 1989–2009. doi: 10.1785/0120140332

Youngs, R. R., & Coppersmith, K. J. (1985). Implications of fault slip rates and earthquake recurrence models to probabilistic seismic hazard estimates. *Bulletin of the Seismological society of America*, *75*(4), 939–964.

Zahran, H. M., Sokolov, V., Youssef, S. E. H., & Alraddadi, W. W. (2015). Preliminary probabilistic seismic hazard assessment for the Kingdom of Saudi Arabia based on combined areal source model: Monte Carlo approach and sensitivity analyses. *Soil Dynamics and Earthquake Engineering*, *77*, 453–468. Retrieved from http://dx.doi.org/10.1016/j.soildyn.2015.06.011 doi: 10.1016/j.soildyn.2015.06.011

Zant, W. (2018). Trains, trade, and transaction costs: How does domestic trade by rail affect market prices of Malawi agricultural commodities? *World Bank Economic Review*, *32*(2), 334–356. doi: 10.1093/wber/lhx011

Zheng, W., Oliva, S. J., Ebinger, C., & Pritchard, M. E. (2020). Aseismic Deformation During the 2014 Mw 5.2 Karonga Earthquake, Malawi, From Satellite Interferometry and Earthquake Source Mechanisms. *Geophysical Research Letters*, *47*(22). doi: 10.1029/2020GL090930

Zhuang, J., Werner, M. J., Harte, D., Hainzl, S., & Zhou, S. (2012). Basic models of seismicity. *Community Online Resource for Statistical Seismicity Analysis*, 2–41. doi: 10.5078/corssa-79905851

Zielke, O., & Strecker, M. R. (2009). Recurrence of large earthquakes in magmatic continental rifts: Insights from a paleoseismic study along the Laikipia-Marmanet fault, Subukia Valley, Kenya rift. *Bulletin of the Seismological Society of America*, *99*(1), 61–70. doi: 10.1785/0120080015

Zöller, G., & Hainzl, S. (2007). Recurrence time distributions of large earthquakes in a stochastic model for coupled fault systems: The role of fault interaction. *Bulletin of the Seismological Society of America*, *97*(5), 1679–1687. doi: 10.1785/0120060262

Statements and Declarations

- **Funding**: This work is funded by the EPSRC-Global Challenges Research Fund PREPARE (EP/P028233/1) and SAFER-PREPARED (part of the 'Innovative data services for aquaculture, seismic resilience and drought adaptation in East Africa' grant; EP/T015462/1) projects.

- **Availability of data and materials**: The Malawi Seismogenic Source Database (MSSD; Williams, Wedmore, Fagereng, et al., 2021a, 2021b) can be accessed through Github at https://github.com/LukeWedmore/malawi_seismogenic_source_database/tree/v1.0 and through Zenodo at: https://doi.org/10.5281/zenodo.5599617. The Malawi Active Fault Database (MAFD; Williams, Wedmore, Scholz, et al., 2021a, 2021b) can be accessed at https://github.com/LukeWedmore/malawi_active_fault_database/tree/v1.0 and https://doi.org/10.5281/zenodo.5507190. The USGS V_{S30} database for Malawi is available from https://earthquake.usgs.gov/data/vs30/

- **Code availability:** MATLAB codes for the generation of the MSSD sources and the probabilistic seismic hazard analysis that is described in this study are available at: https://github.com/jack-williams1/Malawi_PSHA. The stochastic event catalogs and calculated ground motions are also available at: https://zenodo.org/record/6350793#.Yi7DKy0Rpz9, and must be downloaded prior to running the PSHA codes on MATLAB.

- **Authors' contributions:** Conceptualization: all authors-. Methodology: all authors. Software: JW, KG, and RD. Investigation: all authors. Writing - original draft preparation: JW. Writing - reviewing and editing: all authors. Data Curation: JW and LW. Funding acquisition: JB, AF, KG, and MW.

Compliance with ethical standards

- **Conflict of interest**: The authors declare they have no conflict of interest

Appendix A Stochastic Event Catalog Tests

In this section, we perform three tests of the stochastic event catalogs used in the probabilistic seismic hazard analysis (PSHA): (1) if the moment rate ($\dot{M}_0$) of the areal sources in the catalog match the $\dot{M}_0$ derived analytically from their G-R relation (Poggi et al., 2017), (2) if the Combined Catalog matches independent estimates of the geodetic $\dot{M}_0$ in Malawi (Kreemer et al., 2014; Stamps et al., 2018), and (3) quantifying the influence of normal fault obliquity and length-limited source widths on the MSSD-based catalogs $\dot{M}_0$. Results from this testing are described further in Section 4.6 in the main article.

A.1 Areal source catalog validation

To consider whether the event catalog $\dot{M}_0$ of the six areal sources that lie within the region assessed during the PSHA (Fig. 5) matches their $\dot{M}_0$ as derived from their a- and b-value, we first adjust the a-value so that it is consistent with the size of the overlap between the assessed region and the areal source (Table 3). We then discretize this G-R relationship into magnitude bins of 0.01, and calculate the $\dot{M}_0$ of each bin, and for consistency with the event catalogs (Section 4.3), by assuming the magnitude probability distribution follows a truncated exponential relationship (Cosentino et al., 1977). Note, in this $\dot{M}_0$ comparison, events in the areal source catalog with M_W larger than 7.0 were not removed as they are for the actual PSHA (Section 4.3).

Table 3 Gutenberg-Richter relationships and moment rate ($\dot{M}_0$) for areal source zones located within the region assessed during PSHA (Fig. 5).

Source ID (Poggi et al., 2017)	Source Zone	a-value	b-value	M_{Max}	Discretized $\dot{M}_0$ (Nm/yr)	Catalog $\dot{M}_0$ (Nm/yr)
8	Tanganynika	2.9	1.02	7.9	1.2×10^{16}	1.3×10^{16}
9	Rukwa-Malawi	4.7	1.02	7.9	7.3×10^{17}	7.4×10^{17}
13	Kariba–Okavango	2.8	0.99	6.9	4.3×10^{15}	4.5×10^{15}
20	Rovuma Basin	2.6	1.02	6.9	1.8×10^{15}	1.8×10^{15}
N/A	Nyanga	0.4	0.8	7.0	2.6×10^{14}	3.0×10^{14}
N/A	Northeast Mozambique	0.1	0.8	7.0	1.3×10^{14}	1.7×10^{14}
				Total	7.45×10^{17}	7.62×10^{17}

In this analysis, the a-value has been scaled from Table 2 given the overlap between the source zone and assessed region, and events $M_W > 7$ have been removed from the event catalogs.

In all cases, we find a good correlation between the catalog and expected $\dot{M}_0$ (Table 3 and Fig. 17). Discrepancies are higher for the sources with lower moment rates, however, as these sources are inherently only minor contributors to Malawi's seismic hazard, we conclude that the 2 million simulations in the areal source catalogs are of sufficient duration to characterise off-fault seismicity for the PSHA. We note here that the total areal source $\dot{M}_0$ in Malawi (Table 3) is lower than that derived in geodesy or in the MSSD-based catalogs (Fig. 6). We discuss this further in the main article (Section 4.6).

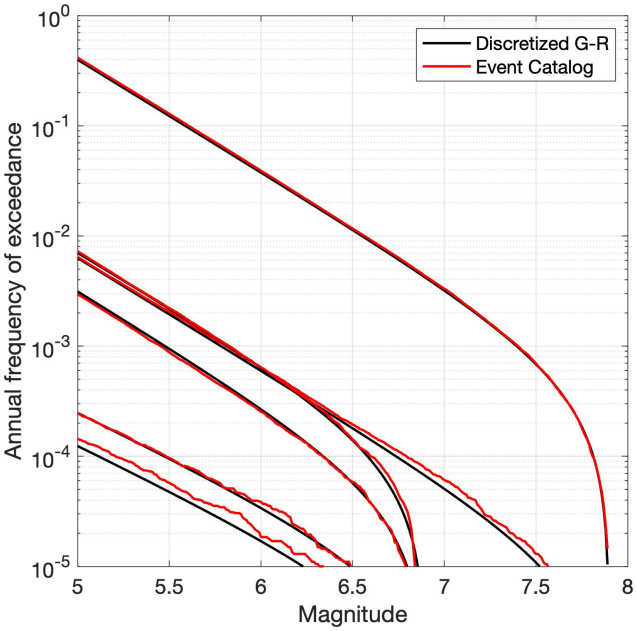

Fig. 17 Discretized and event catalog magnitude frequency distribution (MFD) for the six areal sources from Poggi et al. (2017) that lie within the region assessed for PSHA.

A.2 Analysis of independent geodetic models of Malawi

To derive an independent estimate of the geodetic $\dot{M}_0$ in Malawi, we consider the Global Strain Rate Model (GSRM v.2.1; Kreemer et al., 2014) and the Sub-Saharan African Geodetic Strain Rate Model (SSA-GSRM v.1.0; Stamps et al., 2018). Both models are thus independent from the geodetic constraints used to generate the MSSD-based stochastic event catalogs (Wedmore et al., 2021). We first divide the assessed region shown in Fig. 5 into a grid with intervals of $0.1° \times 0.1°$ longitude and latitude. These grid sizes do not necessarily reflect the true spatial resolution of these models, however, spatial variations in strain rate in regions with few stations are minimised (Stamps et al., 2018). For both models, within each grid i, we first calculate: (1) the second invariant of strain: $(\dot{\epsilon}_{1hi}^2 + \dot{\epsilon}_{2hi}^2)^{0.5}$, where $\dot{\epsilon}_{1hi}$ and $\dot{\epsilon}_{2hi}$ are the two principal strain rates in the horizontal plane of grid i (Kreemer et al., 2014), and (2) the strain rate style: $(\dot{\epsilon}_{1hi} + \dot{\epsilon}_{2hi})/\max(|\dot{\epsilon}_{1hi}|, |\dot{\epsilon}_{2h}|)$ (Kreemer et al., 2014) where a positive style indicates extension and vice versa. We then calculate the moment rate of each grid ($\dot{M}_{0(i)}$) through:

$$\dot{M}_{0(i)} = A_i z \mu \begin{cases} \frac{1}{sin\theta}\dot{\epsilon}_{3i}, \text{ if } \dot{\epsilon}_{2i} < 0 \\ \frac{-1}{sin\theta}\dot{\epsilon}_{1i}, \text{ if } \dot{\epsilon}_{2i} \geq 0 \end{cases} \tag{11}$$

where A_i is the area of each grid, z is the thickness of the seismogenic crust (35 km; Ebinger et al., 2019; Stevens et al., 2021), μ represents the shear modulus (3.3×10^{10} Nm/yr for consistency with; Leonard, 2010), θ is fault dip (53°, section 4.5), and the three principal strain rates of each grid ($\dot{\epsilon}_{1i} \leq \dot{\epsilon}_{2i} \leq \dot{\epsilon}_{3i}$,) are derived by invoking that the vertical strain rate ($\dot{\epsilon}_{rri}$) is a principal strain rate, and that to maintain incompressibility, $\dot{\epsilon}_{1hi} + \dot{\epsilon}_{2hi} + \dot{\epsilon}_{rri} = 0$ (Bird & Liu, 2007; Bird & Kreemer, 2015). Equation 11 is therefore similar to the $\dot{M}_0$ calculation in the seismic hazard inferred from tectonics (SHIFT) model (Bird & Liu, 2007; Bird & Kreemer, 2015), however, we consider the seismic coupling factor (c) separately (Section 4.6) and the assumed 53° dip of faults mean they do not satisfy the criteria that $1/sin(\theta) = 2$. To derive the total geodetic $\dot{M}_0$ across the assessed region, we sum the $\dot{M}_{0(i)}$ from each $0.1° \times 0.1°$ grid.

Malawi can be considered as a region of low magnitude extensional deformation in both of the assessed geodetic models (Fig. 18), which is consistent with the model developed by Wedmore et al. (2021) and observations from seismicity (Ebinger et al., 2019; Stevens et al., 2021). The SSA-GSRM v.1.0 implies greater spatial variability in the magnitude and style of strain in Malawi than the GSRM v.2.1 model. This likely reflects the more comprehensive suite of geodetic data used to develop the SSA-GSRM v.1.0, and although it indicates strike-slip, and even contraction, in regions that have experienced normal fault earthquakes (Biggs et al., 2010; Ebinger et al., 2019), such discrepancies may be reconciled by local strain rotations at the scale of individual faults (Twiss & Unruh, 1998; Williams et al., 2019; Philippon et al., 2015). The MSSD based Combined Catalog $\dot{M}_0$ (1.7×10^{18} Nm/yr, Fig. 6) is approximately intermediate between the total estimates of $\dot{M}_0$ derived from these geodetic models (8.2×10^{17} and 3.5×10^{18} Nm/yr respectively, Fig. 18). This is discussed further in Section 4.6.

A.3 Influence of fault obliquity and width on moment rate estimate

For slip rates in the MSSD estimated through a systems-based approach, the calculation involves projecting a source's dip direction through the regional extension azimuth (Williams, Mdala, et al., 2021). Hence, not all of the geodetic $\dot{M}_0$ assigned to the source is necessarily converted to seismic $\dot{M}_0$. To quantify this, we define the obliquity factor (OF) of MSSD source i, as the ratio of the source's $\dot{M}_0$ relative to its $\dot{M}_0$ if it was optimally oriented to the regional extension direction:

$$OF_i = cos(\theta_i - \phi) \tag{12}$$

where θ_i is the source's strike, and ϕ is the regional extension it is projected through. In some of the MSSD-based catalogs, a source's down-dip is not necessarily extrapolated through the full width of the seismogenic layer, which also implies that the geodetic $\dot{M}_0$ is not all converted to seismicity (Section 4.2). To account for these two effects, we calculated the total $\dot{M}_0$ from all MSSD fault sources on the basis that they extend through the full width of Malawi's

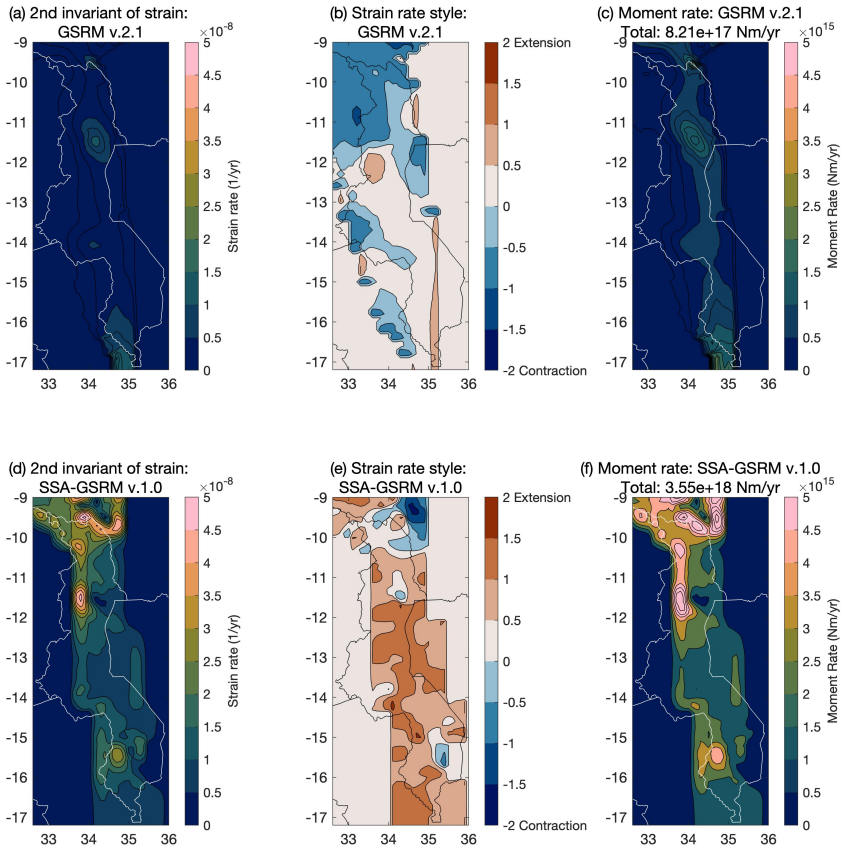

Fig. 18 Analysis of the Global Strain Rate Model (GSRM v.2.1; Kreemer et al., 2014) and and the Sub-Saharan African Geodetic Strain Rate Model (SSA-GSRM v.1.0; Stamps et al., 2018) within the region assessed in the PSHA. Equations for the 2nd invariant of strain, strain rate style, and Moment Rate ($\dot{M}_0$) are given in the text. Total $\dot{M}_0$ refers to the sum of the $\dot{M}_0$ from all $0.1° \times 0.1°$ grids that were assessed.

35 km thick seismogenic layer (Ebinger et al., 2019; Stevens et al., 2021) and that they were all optimally oriented to the regional extension direction (i.e., $OF = 1$). These corrections were not made for the MSSD sources whose downdip extrapolation implies they intersection with another fault (Section 4.5), and for MSSD sources whose slip rate was estimated from offset of the 75 Ka seismic reflection (Shillington et al., 2020).

The total $\dot{M}_0$ of all MSSD fault sources, given corrections for fault obliquity and downdip extent is 1.88×10^{18} Nm/yr. This compares to 1.7×10^{18} Nm/yr for the Combined Catalog (Fig. 6), which incorporates MSSD and areal source seismicity. The difference between these $\dot{M}_0$ estimates indicates that

the inclusion of areal sources does not compensate for the geodetic $\dot{M}_0$ that is lost due to normal fault obliquity and limited down-dip extent. Hence, the Combined Catalog is consistent with a small proportion of aseismic moment release in Malawi (Section 4.6; Zheng et al., 2020) .

Appendix B Supplementary Figures

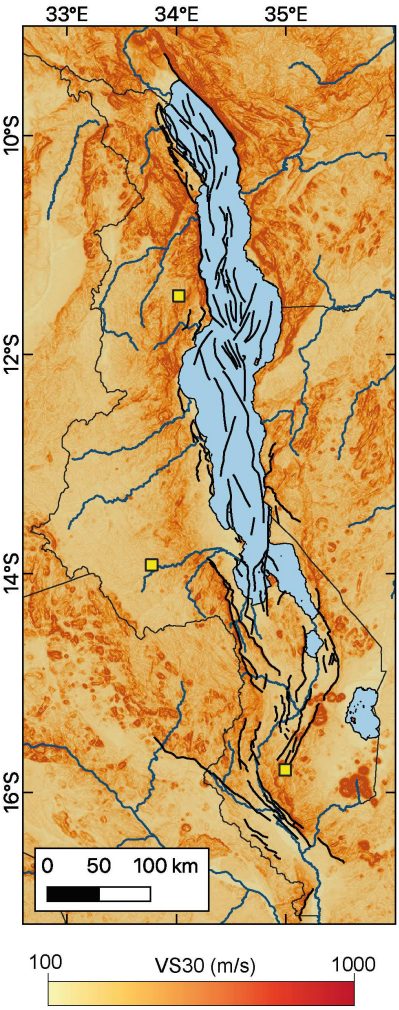

Fig. 19 V_{S30} values in Malawi as derived from using a slope-based proxy (Wald & Allen, 2007), and used in the USGS V_{S30} database (https://earthquake.usgs.gov/data/vs30/). Black lines depict the Malawi Active Fault Database (Williams, Wedmore, Scholz, et al., 2021a) and yellow squares depict the locations for the site-specific PSHA.

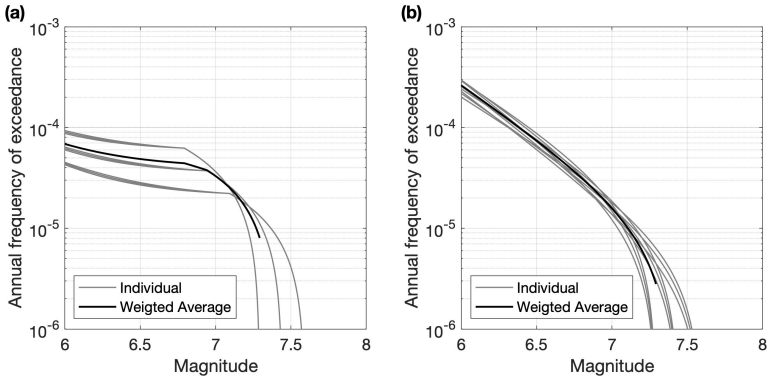

Fig. 20 Nine theoretical magnitude-recurrence curves for the Chingale Step Fault for (a) characteristic and (b) Gutenberg-Richter (G-R) type seismicity under the MSSD-adapted approach (Youngs & Coppersmith, 1985). Each curve considers a different b-value and M_{Max} combination, and is assigned a weighting as described in Section 4.2 and Fig. 2. These weightings are then applied when calculating the weighted average curve.

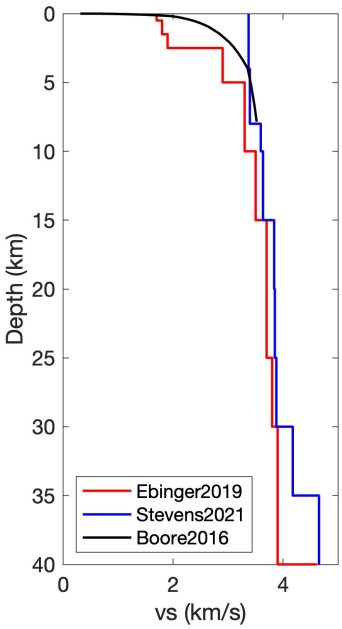

Fig. 21 1D seismic velocity models previously derived in northern (Ebinger et al., 2019) and southern (Stevens et al., 2021) Malawi from short-term seismic deployments. For context the velocity model for the generic rock site from Boore (2016) is also shown for depths 0-8 km.

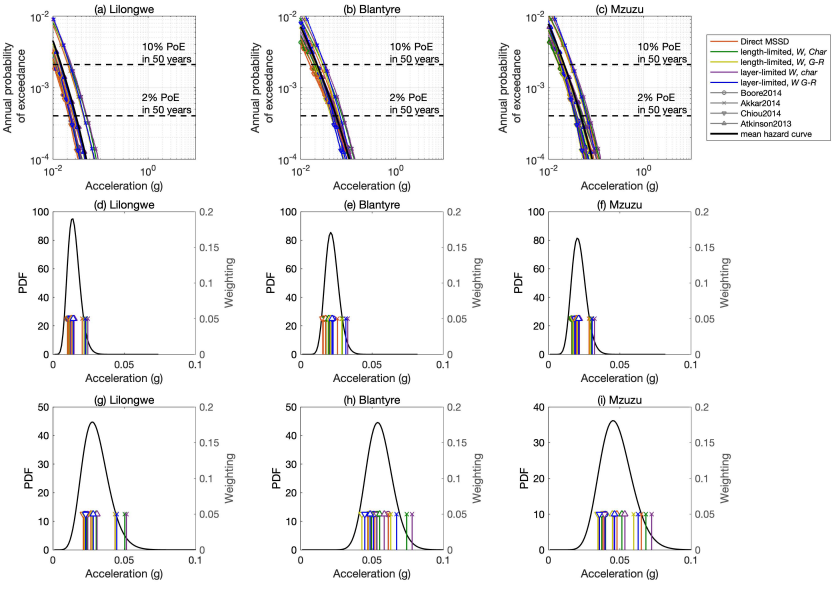

Fig. 22 (a-c) Seismic hazard curves as shown in Fig. 11 but for a Spectral Acceleration of 3 s. In addition, we show the mean value and Beta distribution that may be fitted to these values for (d-f) 10% PoE in 50 years, and (g-i) 2% PoE in 50 years. Note line colors represent different event catalogs, and symbols represent different GMMs. For V_{S30} value of 760 m/s.

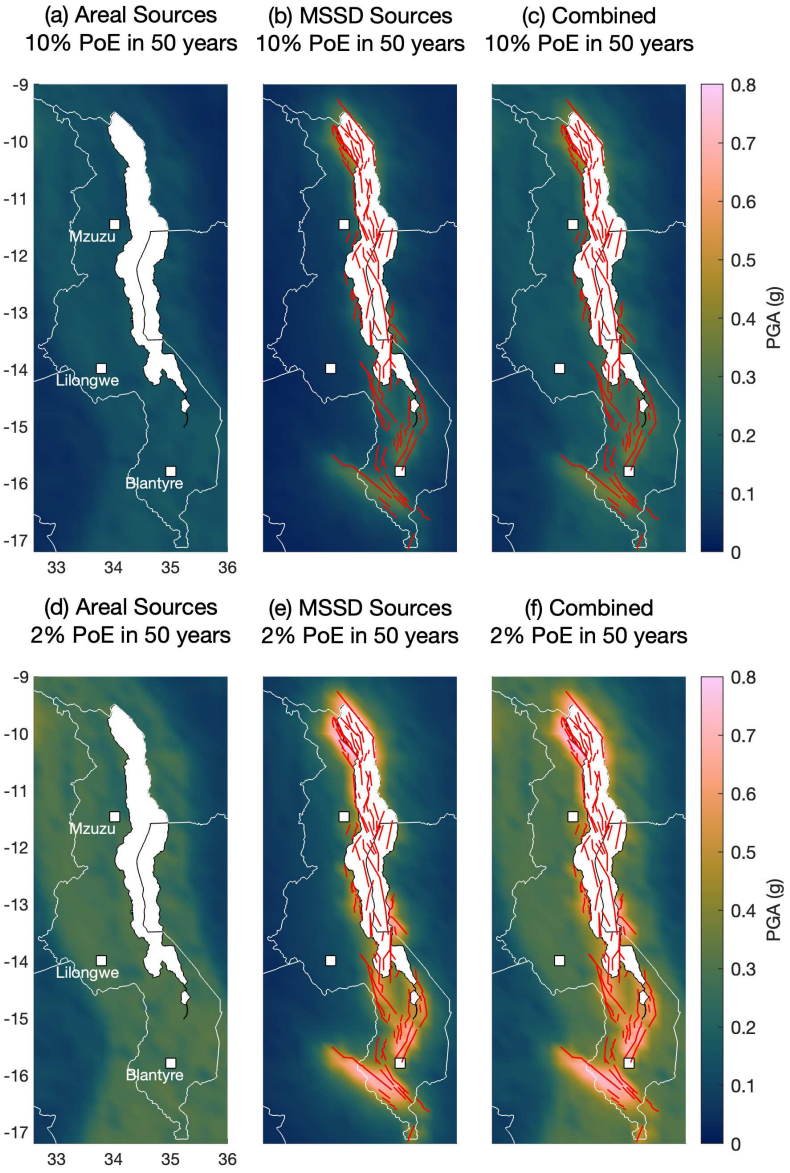

Fig. 23 Equivalent to Fig. 14 with peak ground acceleration (PGA) seismic hazard maps for Malawi, but using the USGS V_{S30} values (Fig. 19; Wald & Allen, 2007). Maps (a)-(c) are for 10% PoE in 50 years, and (d)-(f) 2% PoE in 50 years. Figure is arranged so each column represents a different catalog. Red lines depict the MSSD fault sources (Williams, Wedmore, Fagereng, et al., 2021a).